Progress in Oceanography 214 (2023) 103031

Contents lists available at ScienceDirect

Progress in Oceanography

journal homepage: www.elsevier.com/locate/pocean

Tidal to decadal scale hydrodynamics at two contrasting cold-water coral sites in the Northeast Atlantic

Christian Mohn [a,*], Jørgen L.S. Hansen [a], Marina Carreiro-Silva [b], Stuart A. Cunningham [c], Evert de Froe [d], Carlos Dominguez-Carrió [b], Stefan Gary [c], Ronnie N. Glud [e,f,g], Cordula Göke [a], Clare Johnson [c], Telmo Morato [b], Eva Friis Møller [a], Lorenzo Rovelli [h], Kirstin Schulz [i], Karline Soetaert [j], Anna van der Kaaden [j], Dick van Oevelen [j]

[a] Department of Ecoscience, Aarhus University, Roskilde, Denmark
[b] Instituto de Investigação em Ciências do Mar - Okeanos, Universidade dos Açores, Horta, Portugal
[c] Scottish Association for Marine Science, Oban, United Kingdom
[d] Department of Ocean Systems, Royal Netherlands Institute for Sea Research (NIOZ), Den Burg, Netherlands
[e] HADAL & Nordcee, Department of Biology, University of Southern Denmark, 5230 Odense M, Denmark
[f] Danish Institute of Advanced Study – DIAS, University of Southern Denmark, 5230 Odense M, Denmark
[g] Department of Ocean and Environmental Sciences, Tokyo University of Marine Science and Technology, 108-8477 Tokyo, Japan
[h] iES – Institute for Environmental Sciences, University of Koblenz-Landau, 76829 Landau, Germany
[i] Oden Institute for Computational Engineering and Sciences, The University of Texas at Austin, Austin, TX, USA
[j] Department of Estuarine & Delta Systems, Royal Netherlands Institute for Sea Research (NIOZ), Yerseke, Netherlands

A B S T R A C T

Cold-water corals (CWCs) thrive in areas with complex and rough topography favoring the development of highly diverse benthic communities. Several biotic and abiotic factors including organic matter supply, temperature, bottom roughness and currents are important drivers of ecosystem structure and functioning in deep-sea environments at different spatial and temporal scales. Little is known, however, how basin-scale changes in the ocean climate affect these drivers at local scales. Here, we use high-resolution implementations of the hydrodynamic model ROMS-AGRIF for estimating characteristic spatial and temporal scales of local hydrodynamics in response to variations of basin-scale currents imposed by distinct changes of the Atlantic Meridional Overturning Circulation (AMOC) in the past century. We focus on two CWC communities on the SE Rockall Bank slope and at Condor Seamount. We considered two contrasting AMOC states that were identified from the 1958–2009 hindcast of the 1/20° resolution VIKING20 North Atlantic basin-scale ocean circulation model and used as boundary conditions for the high-resolution local area models. At SE Rockall Bank, variability of near-bottom currents in both regions was largely dominated by tidal dynamics, but strongly modified by AMOC induced basin-scale variations of water mass properties and bottom currents. During strong AMOC years, waters in the main CWC depth corridor (600–1200 m) were cooler and less saline but were dominated by stronger bottom currents when compared with conditions during weak AMOC years. At Condor Seamount, bottom currents were largely unaffected by AMOC related changes close to the summit at water depths < 400 m. Kinetic energy dissipation rates derived from the 3D near-bottom velocity field appeared to positively relate with the in-situ CWC distribution. Kinetic energy dissipation is therefore proposed as a mechanistic descriptor of CWC presence as it provides a more mechanistic view of hydrodynamics driving organic matter supply to filter and suspension-feeding communities.

1. Introduction

The distribution of benthic communities and their associated ecosystem processes are constrained by the physical and chemical properties of the overlaying water masses. In particular, suspension-feeding organisms (such as CWC) cannot themselves generate a significant feeding current and rely on the physical advection of water masses, which renew their suspended food sources and flush the habitats with fresh oxygenated water (Mienis et al., 2019). Temporal changes in the near-bottom physical environment, as experienced by sessile benthic fauna, occur on different timescales. The characteristic timescale of changes in currents and other physical parameters may itself be an important driver of benthic ecosystem processes, thus shaping the benthic faunal composition. Daily and seasonal variations (e.g., changes in seasonal pycnocline depth and tidal dynamics) influence deep-sea benthic communities (Juva et al., 2020; van der Kaaden et al., 2021). The effect of climate change remains however less explored and understood but is expected to cause profound changes of deep-sea

* Corresponding author.
E-mail address: chmo@ecos.au.dk (C. Mohn).

https://doi.org/10.1016/j.pocean.2023.103031
Received 28 July 2022; Received in revised form 24 March 2023; Accepted 24 April 2023
Available online 26 April 2023

ecosystems (Sweetman et al., 2017). In the deep-sea, the spectrum of temporal variability in currents is dominated by short-term predictable cycles driven by tides as well as long-term, multi-annual changes over geological timescales of tens to hundreds of thousands of years (Colin et al., 2010, 2019). At intermediate (decadal) timescales, the possible role of basin-wide ocean current systems on deep-sea variability remains unclear. This lack of knowledge mostly responds to time-limited field observations (not lasting long enough), and to paleo records, which are too coarse in resolution to resolve the decadal time scale. Therefore, it is currently unknown how this intermediate decadal variability in basin-wide oceanic currents could affect benthic communities such as those dominated by CWC reefs and deep-sea sponges.

Basin-scale variability of physical properties in the North Atlantic often follows periodic decadal patterns, identified, and quantified by ocean climate indices, which describe characteristic alternating states in the circulation systems (Johnson et al., 2020). Amongst these, the AMOC represents the strength of the overturning circulation through winter convection in the North Atlantic and it is an important indicator for the conversion of upper waters to dense intermediate and deep waters (Frajka-Williams et al., 2019; Petit et al., 2020). The AMOC is characterized by periods of stronger and weaker states that are closely linked to the dynamics of the overall North Atlantic gyre system. Another important index is the subpolar gyre index (SPG) describing variations in strength and lateral extension of the subpolar gyre across the northern North Atlantic (Hátún et al., 2005).

In the North Atlantic, the strongest AMOC end members generally occur south of 40°N where negative phases were predficted from the early 1960s to the late 1980s followed by a largely positive phase since the late 1980s (Böning et al., 2016). North of 40°N, at mid and high latitudes, AMOC variability is more pronounced on shorter time scales and is occasionally out of phase with the subtropical and tropical part of the Atlantic. Hindcast model simulations indicate that the weakest and strongest AMOC states in the last decades appeared in 1978–1981 and 1992–1995, respectively. During these two periods, AMOC phases were more or less synchronized across latitudes from 10°N to 60°N, including at the two CWC areas studied here: the Rockall Bank (55°N) and Condor Seamount (38°N). In recent years (from 1999 onwards) the AMOC has followed a period of overall weakening, also at these two study sites (Srokosz and Bryden, 2015).

The AMOC phases and other changes in the North Atlantic gyre system cause a cascade of effects across all trophic levels of the North Atlantic upper water ecosystems (Hátún et al., 2009a) including important commercial fish stocks (Hátún et al., 2009) and seabirds (Hátún et al., 2017). Changes in the basin-scale circulation and water mass properties propagate to the deep sea and may affect ecosystem processes in different ways (Puerta et al., 2020; Morato et al., 2020; O'Brien et al., 2021). Several studies have highlighted linkages between alternating phases of ocean current systems to long-term changes in the growth rates and elemental composition of CWC reefs during Holocene (e.g., Montero-Serrano et al., 2011; Dubois-Dauphin et al., 2019). Colin et al. (2010, 2019) analyzed stable neodymium isotope composition in *Desmophyllum pertusum* (*D. pertusum* hereafter) reefs to fingerprint the dynamics of the water masses at the reefs during the Holocene. Likewise, Bonneau et al. (2018) was able to link growth rates of *D. pertusum* reefs and carbonate mounds to the long-term evolution of Atlantic Ocean indices during the Holocene. This latter study suggested that the relationship between long-term effects of Atlantic Ocean indices on coral growth was due to increased food availability during periods of strong currents. Although there is discussion regarding the classification, we follow WoRMS (dd 21-07-2022) and use the accepted name *D. pertusum* (formely named *Lophelia pertusa*) and remark specifically that we refer to the colonial form of *D. pertusum*.

Observational and experimental studies have shown that an important environmental constraint on CWC growth is the supply of labile suspended particulate organic matter (e.g., Davies et al., 2009; Eisele et al., 2011). In general, food supply to suspension feeding organisms depends on the availability of food, as given by the concentration of suspended food items, and on the supply rate to the benthic species. Thus, food supply is directly related to hydrodynamics (e.g., current speed and turbulence), bringing the food items in contact with the benthic organisms (Shimeta and Jumars, 1991). Although organic matter concentration in the deep-sea is related to the overall export from the productive surface layers of the ocean, there can be considerable local variation based on how efficient the fauna is in clearing the water, which in turn depends on bottom roughness influencing local near-bed currents and vertical mixing (Mohn et al. 2014; Cyr et al., 2016; Soetaert et al., 2016). Strong hydrodynamic activity may even cause resuspension of organic material, thereby further increasing food concentration (Davies et al., 2009). The effect of near-field current speeds on CWC feeding performance on plankton is documented in laboratory (Purser et al., 2010; Orejas et al., 2016; Hennige et al., 2021) and in situ experiments, where observations of the filtration activity of individual *D. pertusum* polyps responded to tidal rhythms of near-bed currents (Osterloff et al., 2019). The significance of currents has also been inferred by comparing the spatial distributions of *D. pertusum* reefs and near-bed current speeds (e.g., Rengstorf et al., 2014). Model studies suggest that episodically intensified internal tidal mixing has the potential of mixing productive surface waters down to a 600 m deep summit of a carbonate mound, thereby transporting fresh organic matter to the deep-sea benthos (Soetaert et al., 2016). In fact, van der Kaaden et al. (2021) found that the size of the carbonate mounds hosting corals controls mixing intensity and thus food supply. Likewise current speed has repeatedly emerged as an important factor in the modelling of suitable habitats of *D. pertusum* (Davies et al., 2008; Rengstorf et al., 2014; De Clippele et al., 2017). Within areas of *D. pertusum* reefs, where currents predominantly move in one direction, largest colony growth rates were recorded upstream against the dominating current (Buhl-Mortensen et al., 2010; Mienis et al., 2014), which may be a response to a shading-off of the food flux for the down-stream corals (Wagner et al., 2011; Mienis et al., 2019). Competition for accessing the food flux of the current is even evident within colonies of *D. pertusum* even at the cm-scale, with individual polyps in the colony orientated against the dominant current (Purser et al., 2010; Orejas et al., 2016).

By acknowledging the growing evidence from field and laboratory studies of the interplay between CWC distribution and the ambient hydrodynamic environment across different spatial and temporal scales, we focus on model-based estimates of local hydrodynamics at intermediate scales with respect to both time and space. Spatially, we will aim at resolving processes at the 100–1000 m scale. Temporally, we focus on changes in the physical environment at the decadal time scale related to basin-scale variations driven by the state of the AMOC. As climate change may affect AMOC, modelling of decadal time scales may therefore also include more general predictions of climate change effects on deep-sea ecosystems. We use the existing low-resolution basin-wide North Atlantic model, VIKING20 to produce boundary conditions for two high-resolution implementations of the ROMS-AGRIF model, which covers the southeastern sector of Rockall Bank and the entire Condor Seamount area. We analyze how characteristic basin-wide AMOC anomalies propagate into tidal driven dynamics of near-bottom currents at these two sites to study how this could modify the local physical environment of the deep-sea benthos. Furthermore, in order to embrace the various fine scale hydrodynamic processes that may be influenced by the AMOC state, we calculate and map kinetic energy dissipation rates. Energy conversion from basin-scale geostrophic currents and barotropic tidal currents to internal tides and to higher frequency and turbulent motions generates energetic internal motions in the deep ocean interior at small dissipation length scales (Ledwell et al., 2000; Merrifield et al., 2001; Nikurashin et al., 2013). Modelling of barotropic tides have suggested that 25–30 % of the global tidal kinetic energy dissipation occurs in the deep ocean (Egbert and Ray, 2000; Nikurashin et al., 2013). Enhanced kinetic energy dissipation in the model by Egbert and Ray (2000) was found at topographic features, suggesting that tidal energy

conversion from barotropic to baroclinic tides is most energetic over rough, smaller scale topography (Merrifield et al., 2001). We propose kinetic energy dissipation as a predictive proxy for food accessibility and suitable habitat of CWC in the deep-sea expanding on considerations and methods described in van der Kaaden et al. (2021). Kinetic energy dissipation rates can be calculated with a spatial resolution characteristic of the model domain and changes of the near-bottom flow dynamics induced by AMOC states can thus be mapped. We will test how well distributions of kinetic energy dissipation under the different AMOC states match the distribution of CWCs at SE Rockall Bank.

2. Study sites

2.1. Southeast (SE) Rockall Bank

The Rockall Bank forms the western boundary of the Rockall Trough, a semi-enclosed basin west of the European continental shelf, located approximately 400 km NW of Ireland (Fig. 1 a). On the southeastern slope of the Rockall Bank, numerous coral-capped carbonate mounds are present between 500 and 1000 m water depth forming the Logachev mound province (Kenyon et al., 2003; Mienis et al., 2006). These carbonate mounds can be ten to hundreds of meters high, several kilometers wide, and are composed of dead coral fragments and sediment (Mienis et al., 2009). Benthic communities living on and around the mound summits consist of the corals *D. pertusum* and *Madrepora oculata* with a high number of associated macrofauna species including

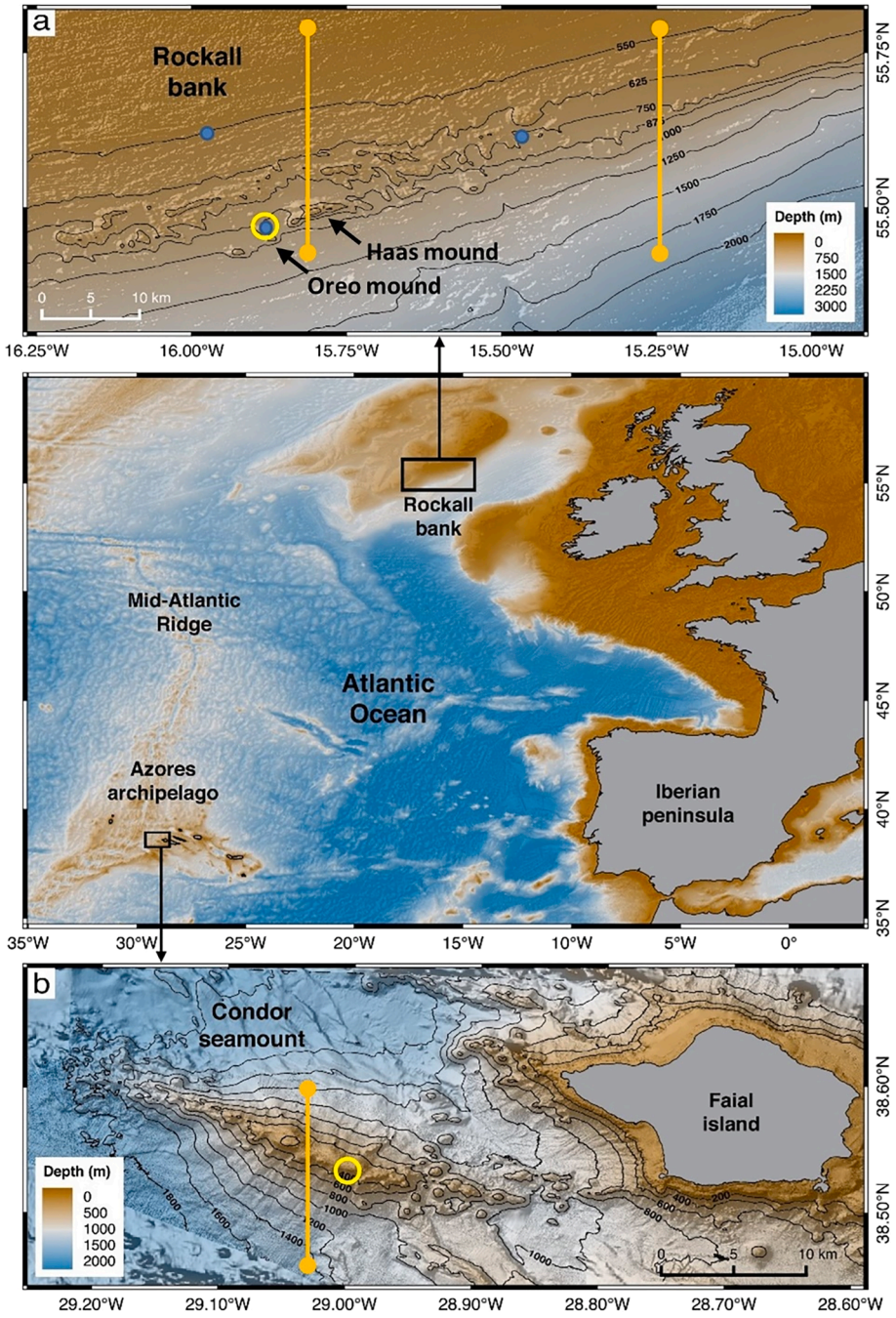

Fig. 1. Bathymetry of the wider study region and local embedded ROMS-AGRIF model implementations. (a) Logachev mound province (SE Rockall Bank) with locations (blue bullet points) of current meter moorings used for model validation, (b) Condor Seamount (Azores). The horizontal resolution of each embedded grid is 250 m. The corresponding horizontal resolution of the parent grids (not shown in this figure) is 750 m. In (b) only part of the model domain is shown. Please note that the two model grids are not equally scaled. The orange lines indicate locations of transects shown in Fig. 14. The yellow circles show positions, where timeseries of modelled currents were extracted to calculate power spectra as shown in Fig. 12.

polychaetes, sponges, and crinoids (Van Weering et al., 2003; Van Soest and Lavaleye, 2005; Maier et al., 2021). The general water flow along the SE slope of Rockall Bank is in SW direction driven by a combination of an anticyclonic circulation circumventing Rockall Bank and advection of water masses from the Northern Rockall Trough. Water masses in the upper 600 m consist mainly of Eastern North Atlantic Water (ENAW), which enters the Rockall Trough from the south (McGrath et al., 2012). From the North, Wyville Thomson Overflow Water (WTOW) propagates southwards as a boundary current along the eastern flank of the Rockall Bank, at depths between 600 m and 1200 m (Penny Holliday et al., 2000; Johnson et al., 2010; Schulz et al., 2020). The densest core of WTOW has been reported even deeper at depths between 1200 m and 1500 m (Johnson et al., 2017). Closer to the carbonate mounds ambient bottom water temperatures are typically 7–9 °C, and the mound region is known for distinct tidally generated hydrodynamic features such as energetic internal waves and hydraulic jumps (Mohn et al., 2014; Van Haren et al., 2014; Cyr et al., 2016). The distribution of carbonate mounds along the continental margins of Rockall Bank and Porcupine Bank corresponds to the depth corridor of the permanent thermocline in the NE Atlantic (600–1000 m; White and Dorschel, 2010). In this depth range, the strong density gradients at the base of the permanent thermocline in combination with the steep continental slope support both energetic internal waves and enhanced residual near-bottom currents (White and Dorschel, 2010; Schulz et al., 2020). These dynamic conditions promote stable organic matter supply through along-slope and cross-slope sediment transport (Duineveld et al., 2007; Mienis et al., 2007; Soetaert et al., 2016).

2.2. Condor Seamount

Condor Seamount is an elongated seamount (26 km long, 7.4 km wide) located 100 km east of the Mid-Atlantic Ridge (MAR) and 17 km SW of the island of Faial in the Azores Archipelago (Fig. 1 b). It rises from approximately 1500 m water depth to a narrow summit plateau at an average depth of 185 m. Water masses and currents in the wider Azores region are largely dominated by the Azores Current system and inflow of waters from the subtropical gyre. The Azores Current is one of the most prominent flow systems of the basin-wide circulation in the subtropical Northeast Atlantic. The main current is defined as an up to 150 km wide eastward meandering jet in the upper 1000 m east of the MAR between the Azores and Madeira Island (Klein and Siedler, 1989; Lozier et al., 1995). The current's central axis spans along the 35°–40°N latitude range and is marked by intense mesoscale eddy activity from baroclinic instabilities of the main Azores Current (Barbosa Aguiar et al., 2011). Southwestward propagating Mediterranean Water eddies (Meddies) and their pathways along and across complex topographic features including seamounts dominate deeper waters in the depth range between 800 m and 1500 m (Wang and Dewar, 2003; Bashmachnikov et al., 2009). Water properties around the Azores archipelago are characterized by the influence of three major water masses (Palma et al., 2012), ENACW (Eastern North Atlantic Central Water, temperature range 10–20 °C, salinity range 35.5–36.4), MW (Mediterranean Water, 5–10 °C, salinity range 35.3–35.6) and NADW (North Atlantic Deep Water, 3–5 °C, salinity range 34.9–35.3). The local circulation at Condor Seamount is dominated by different components of tidal and sub-tidal flow generating an anticyclonic Taylor Cap along the upper slopes and cross-isobath flow atop the summit (Bashmachnikov et al., 2013). The stability of the vortex is to a large degree controlled by the variability of the larger scale flow in the immediate far field of the seamount. Periods during which the vortex is absent, are characterized by pronounced short-term variations in the direction of the impinging flow. The anticyclonic vortex is re-established after reconsolidation of the mean flow (Bashmachnikov et al., 2013). Primary productivity is generally low with elevated values in spring locally enhanced in areas with strong upwelling around islands and seamounts (Santos et al., 2013), and thus providing ideal conditions for the growth of filter and suspension-feeding organisms such as octocorals and sponges. Based on historical and present coral records, the Azores have been described to host a particularly high diversity of CWCs with 184 species identified to date (Braga-Henriques et al., 2013; Sampaio et al., 2019). Biogeographically, corals of the Azores have a greater affinity to the Lusitanian-Mediterranean biogeographic region and to a lesser extent to the western North Atlantic. Condor Seamount hosts habitats of high conservation importance including coral gardens and deep-sea sponge aggregations (Tempera et al., 2012). Dense aggregations of octocorals are commonly observed on the seamount summit, at water depths <287 m (Tempera et al., 2012). The gorgonians *Viminella flagellum* and *Dentomuricea c.f. meteor* are the most common and abundant coral species of the summit, forming dense patches alongside the large gorgonians *Callogorgia verticillata* and *Paracalyptrophora josephinae*, the small branching gorgonian of the genus *Acanthogorgia* and hydrarians of the species cf. *Polyplumaria flabellate* and cf. *Lytocarpia myriophyllum* (Tempera et al., 2012).

3. Material and methods

3.1. High-resolution local area model implementations (ROMS-AGRIF)

We use the Regional Ocean Modelling System with grid refinement (ROMS-AGRIF) to describe near-bottom dynamics in contrasting AMOC states for two areas with fundamentally different bathymetric landscapes. ROMS-AGRIF is a 3-D, free surface, finite difference, primitive equation model employing orthogonal curvilinear coordinates on a staggered Arakawa C-grid in the horizontal and stretched terrain-following sigma coordinates (s-coordinates) in the vertical (Shchepetkin and McWilliams, 2005). The model version in this study includes the one-way grid nesting package AGRIF Fortran (Adaptive Grid Refinement in Fortran; Debreu et al., 2008), permitting simultaneous downscaled simulations across multiple numerical grids. The ROMS implementations of the two study areas largely follow the setup described in Mohn et al. (2014). We use a high resolution (250 m) small model domain (child grid) embedded in a lower resolution (750 m) larger model domain (parent grid) for each case study area (Fig. 1, Table 1). All model domains have 32 terrain-following vertical layers with higher resolution close to the surface (stretching parameter θ_s = 3.4) and bottom ($\theta_b = 1.0$). ROMS uses a third-order upwind scheme for advection of momentum and tracers. Sub-grid scale vertical mixing processes are parameterized by a non-local K-profile planetary (KPP) boundary layer scheme (Large et al., 1994; Durski et al., 2004). The parent grids receive physical properties from VIKING20 five-day averages of baroclinic velocities, temperature, and salinity across the open lateral boundaries. The OSU inverse tidal model provides instantaneous sea surface height and barotropic velocities for 10 tidal constituents (Egbert and Erofeeva, 2002), through radiation terms along the open lateral boundaries. Local solutions of water mass properties and currents from the parent grids are transferred to the child grids at every time step using the same open boundary radiation terms. Explicit lateral viscosity

Table 1
Grid metrics for local high-resolution ROMS-AGRIF model implementations.

Grid geometry	Rockall Bank (parent grid)	Rockall Bank (child grid)	Condor Seamount (parent grid)	Condor Seamount (child grid)
Horizontal resolution (m)	750	250	750	250
Grid size (km)	191 × 187	85 × 57	105 × 110	66 × 63
Number of grid points	250 × 250	338 × 230	134 × 142	254 × 242
Longitude range (° W)	−17 to −14	−16.276 to −14.928	−29.6 to −28.4	−29.327 to −28.568
Latitude range (° N)	54.815 to 56.50	55.346 to 55.864	38 to 39	38.218 to 38.784

is zero everywhere in the models except in 2400 m (parent grids) and 800 m (child grids) wide sponge layers to reduce numerical instabilities along the open boundaries. COADS (Comprehensive Ocean-Atmosphere Data Set, 0.5 × 0.5° spatial resolution) data was used as background atmospheric forcing at the free surface. The total simulation time was set to three years for each AMOC period representing conditions of weak (1978–1980) and strong (1992–1994) AMOC state. The largest model time step is 120 s, which is sufficient to capture tidal dynamics as an important physical driver at these sites.

3.2. Basin-scale variability (VIKING20)

The VIKING20 model is an ocean-only nest of the polar and sub-polar North Atlantic embedded in the global ocean general circulation and sea-ice model ORCA025 (1/4° resolution) using the AGRIF package for adaptive grid nesting (Debreu et al 2008). The VIKING20 model is eddy-resolving with a spatial resolution of 1/20° with prescribed CORE2 atmosphere and covers the North Atlantic in the latitudinal range 30°N–80°N (Böning et al., 2016). The basin-scale circulation in the upper and deep waters of the North Atlantic follows multi-annual spatial and temporal patterns, which can be described in ocean climate indices (Johnson et al., 2020). We used two of the most used indices as a basis for our analysis, AMOC and SPG. The AMOC represents the strength of the overturning circulation in the northern North Atlantic and is an indicator for the conversion of upper waters to dense intermediate and deep waters. The SPG index describes dynamic relationships between the salinity of the poleward Atlantic Inflow and the strength and extension of the subpolar gyre from analysis of sea surface height (SSH) and salinity anomalies (Hátún et al., 2005; Johnson et al., 2020; and references therein). In the North Atlantic, several studies suggest a link between the AMOC and SPG. Phases of positive AMOC correspond to phases of strong eastward extension of the SPG and negative salinity anomalies (Hátún et al., 2005; Johnson et al., 2020). South of 40°N, periods of weak AMOC have been identified from the early 1960s to the late 1980s and strong AMOC since the late 1980s. The most pronounced end members appear in two periods, 1978–1981 (weak AMOC) and 1992–1999 (strong AMOC) respectively (Fig. 2 a) based on results in Böning et al. (2016). North of 40°N, at mid and high latitudes, AMOC variations are occasionally out of phase with conditions in the subtropical and tropical Atlantic. However, the most intense weak and strong AMOC states are also predicted for the late 1970s and early 1990s (Fig. 2 a). EOF (Empirical Orthogonal Functions) analysis of the basin wide SSH from the VIKING20 model shows that the two leading EOF modes explain 28 % of the total variance of the 50 year data set (1959–2009). The spatial and temporal distribution of the second EOF mode represents the spatial extension of the large-scale N-Atlantic gyre systems (Fig. 2 b). In general, twentieth century trends in the SPG variability are considered exceptional exceeding the range of variability during the last 10,000 years and suggesting a strong shift in the dynamics of the SPG circulation (Spooner et al., 2020). In our simulations, three years of VIKING20 model data from each AMOC end member (1978–1980, 1992–1994) was extracted as boundary conditions for the local area model implementations described in the previous section.

3.3. Model validation

The main objective of the high-resolution model simulations was to assess the propagation of water mass properties and currents during contrasting AMOC conditions in tidally dominated CWC areas. We did not initially prioritize data availability for model validation. Validation of the model physics is therefore not straightforward since well-established datasets for the two AMOC periods in the areas under consideration do not exist. To compensate for this lack of in-situ data in time, modern day observations combined from several research campaigns from SE Rockall Bank were compared with modelled data from a period with a matching AMOC state (Table 2). Corresponding observations from Condor Seamount were not accessible to the public at the time this study was completed.

From SE Rockall Bank, four data sets were available from three different locations. The first data set was collected during a 6-week deployment of two recording Aanderaa RCM7 current meters in August and September 2000. Current velocities were recorded at 20-minute intervals at discrete depths at 10 and 150 m above the bottom in the NE Logachev province (White et al., 2007). The second data set was recorded with long-range Acoustic Doppler Current Profilers (ADCPs), which were deployed from May 2017 to May 2018 (Schulz et al., 2020). One mooring line was deployed on the upper slope of SE Rockall Bank and a second one above Oreo mound (Fig. 1). On both moorings, an upward looking 75 kHz ADCP (RDI Workhorse) was installed on a buoyancy unit, at a height of 41 m above the seabed. Profiles of current velocities were stored every 20 min, with a vertical resolution of 4 m (Rockall Bank) and 8 m (Oreo mound). The data was internally converted into ENU (East-North-Up) coordinates. Table 2 summarizes the mooring locations, sampling periods, and respective bottom and instrument depths. Both datasets were recorded close to periods of reported AMOC weakening starting in the early 2000 s (Srokosz and Bryden, 2015) and were compared with modelled currents from corresponding periods of weak AMOC state for the years 1978–1980. As the most pronounced end members in their respective AMOC periods, the years 1979 and 1993 were chosen for model validation and later analysis of seasonal and interdecadal variability (Fig. 2a). To assess statistical model performance, we calculated a cost function (CF) providing a measure of the goodness of fit between model data and observations,

$$CF = \frac{\sum |M - D|}{N\sigma_D}$$

where D is the observed data, M the corresponding model value, N is the number of observed data points and σ_D is the standard deviation of data (Radach and Moll, 2006; Wan et al., 2012). Observations and model

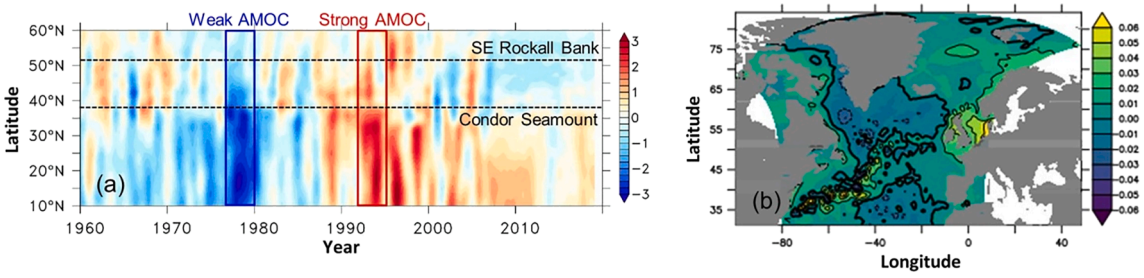

Fig. 2. (a) VIKING20 basin wide AMOC anomalies reproduced from Böning et al. (2016) from their supplementary information, Fig. S4c (a). Periods of weak (1978–1981) and strong (1992–1999) AMOC state are shown across a range of subpolar and subtropical latitudes. Three years during each AMOC end member state were extracted from the VIKING20 data for this study (1978–1980, 1992–1994). Black dashed lines indicate the latitudes of SE Rockall Bank and Condor Seamount, respectively. (b) Spatial eigenfunctions of the second EOF calculated from VIKING20 SSH data for the period 1959–2009.

Table 2
Locations and sampling periods of current measurements used for validation of the SE Rockall Bank model (see Fig. 1 for an overview of station locations).

Location	Longitude (W)	Latitude (N)	Sampling period	Depth of seabed	Instrument depth	Data reference
SE Rockall Bank (Logachev province)	15°27.7′	55°36.4′	02-Aug to 15-Sep 2000	818	808	White et al. (2007)
SE Rockall Bank (Logachev province)	15°27.7′	55°36.4′	02-Aug 2000 to 15-Sep 2000	818	668	White et al. (2007)
SE Rockall Bank (Oreo mound)	15°51.968′	55°27.048′	09-May 2017 to 05-May 2018	781	41 m above seabed	Schulz et al. (2020)
SE Rockall Bank (upper slope)	15°55.839′	55°38.448′	02-May 2017 to 05-May 2018	507	41 m above seabed	Schulz et al. (2020)

data were sub-sampled at 3-hour intervals. CF is one of several score-based measures used for model skill assessments ranking model performance as very good (CF < 1), good (CF = 1–2), reasonable (CF = 2–3) or poor (CF > 3).

3.4. Model data analysis

Time-averaged composites (3-year average of each AMOC state) and time series of near-bottom potential temperature (θ), salinity (S) and currents from the ROMS-AGRIF model output were compared between periods of weak and strong AMOC state in each study area. In addition to mapping the domain-wide time-averaged distributions, the seasonal evolution of θ, S and current magnitude in locations with steep terrain gradients was analysed from daily averaged model data time series. For this calculation, only areas inside prominent coral corridors at bottom depths 600 m < H < 1200 m (SE Rockall Bank) and H < 400 m (Condor Seamount summit area) were considered. Power spectra of 3-hourly instantaneous modelled near-bottom currents were calculated to assess the evolution of higher frequency currents in different seasons and AMOC states at two single locations with known CWC presence (see Fig. 1).

We hypothesize that topographically enhanced transfer of kinetic energy and conversion towards higher frequency motions is potentially important for sessile benthic organisms as a mechanism of food supply. Hence, we use kinetic energy dissipation as a hydrodynamic indicator to predict suitable habitat for suspension feeders at the seafloor (see also; van der Kaaden et al., 2021). In our analysis, we estimate kinetic energy dissipation rates from daily averages of the modelled 3D velocity field expressed as in Nikurashin et al. (2013),

$$\varepsilon = \rho \bullet A_h \left[\left(\frac{\partial U}{\partial x}\right) \bullet \left(\frac{\partial U}{\partial x}\right) + \left(\frac{\partial U}{\partial y}\right) \bullet \left(\frac{\partial U}{\partial y}\right) \right] + \rho \bullet A_v \left[\left(\frac{\partial U}{\partial z}\right) \bullet \left(\frac{\partial U}{\partial z}\right) \right]$$

where horizontal viscosity $A_h = 1\ m^2\ s^{-1}$ and vertical viscosity $A_v = 10^{-3}\ m^2\ s^{-1}$ consider the large aspect ratio between horizontal and vertical exchange of momentum, ρ = density of seawater (kg m^{-3}) calculated from the modelled temperature and salinity fields, U (u, v, w) is the 3D velocity vector (m s^{-1}) in directions east (x), north (y) and up (z).

4. Results

4.1. Model-data comparison

The observed current velocities for August/September 2000 at the Logachev mooring site (SE Rockall Bank) at 10 m and 150 m above the bottom are shown in Fig. 3 a, b. The best agreement between model and observations was found in the near-bottom layer, where flow dynamics and variability are dominated by tidal dynamics. In this layer, modelled current velocities extracted at the nearest grid point and closest depth of the Logachev mooring agree well with observations, both in velocity magnitude and orientation (Fig. 3 a). Higher frequency currents were strongest in the semi-diurnal and diurnal tidal bands, as diurnal oscillations are strongly intensified near the bottom and during spring tide with maximum velocities up to 0.4 m s^{-1} (Fig. 3 a; spectral analysis in supplementary Fig. S1 a). At 150 m above the bottom, the 1979 model results generally underestimate observed 2000 currents in the E-W direction, whereas the model reproduces N-S current velocities rather

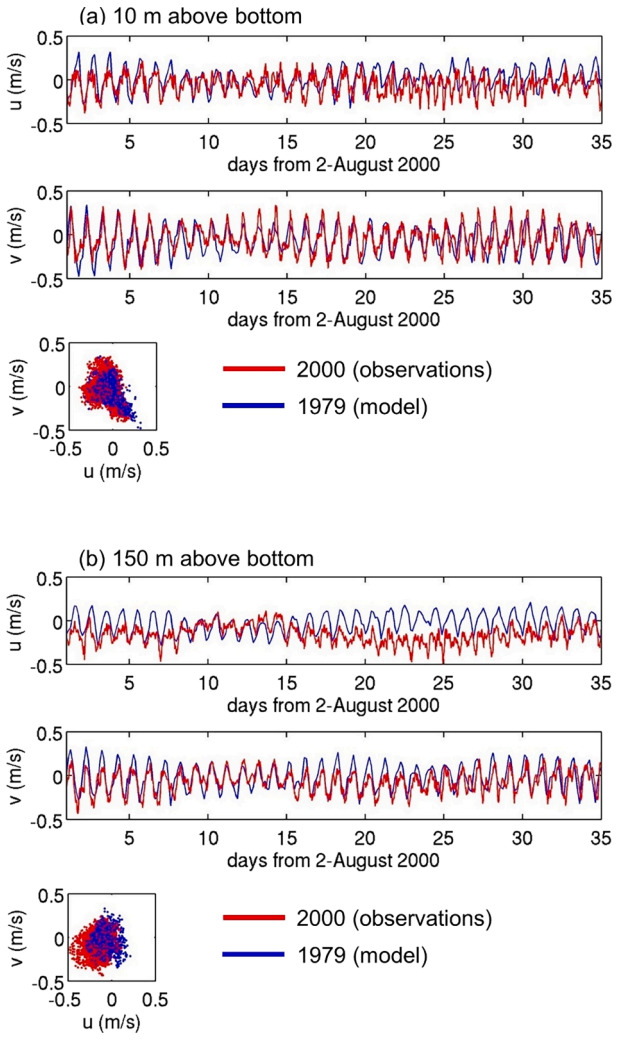

Fig. 3. Time series (20-minute intervals, 35 days) of current velocities recorded by moored current meters in August/September 2000 in the eastern Logachev province (red lines and scatter points; White et al., 2007). Corresponding modelled current velocities (August/September 3-hourly output from the 1979 simulations) are displayed as blue lines and blue scatter points (see Table 2 for more information about mooring location and sampling period). (a) 10 m above the seafloor, (b) 150 m above the seafloor. Please note supplementary Fig. S1 for a more detailed analysis of current spectra.

accurately (Fig. 3 b). Spectral analysis of current magnitude shows again strongly enhanced diurnal oscillations as the dominant signal in both observations and model output (supplementary Fig. S1 b). Daily mean, depth-averaged current velocities from the long-term 2017/2018 ADCP deployments in SE Rockall Bank are shown in Fig. 4. Maximum current velocities were 0.2 m s^{-1} at both locations with a more pronounced seasonality at the deeper Oreo mound mooring. Observations were compared with corresponding model data from the weak AMOC years 1979/1980. Major variability patterns at modelled locations agree well with observed currents, particularly between May and November 2017

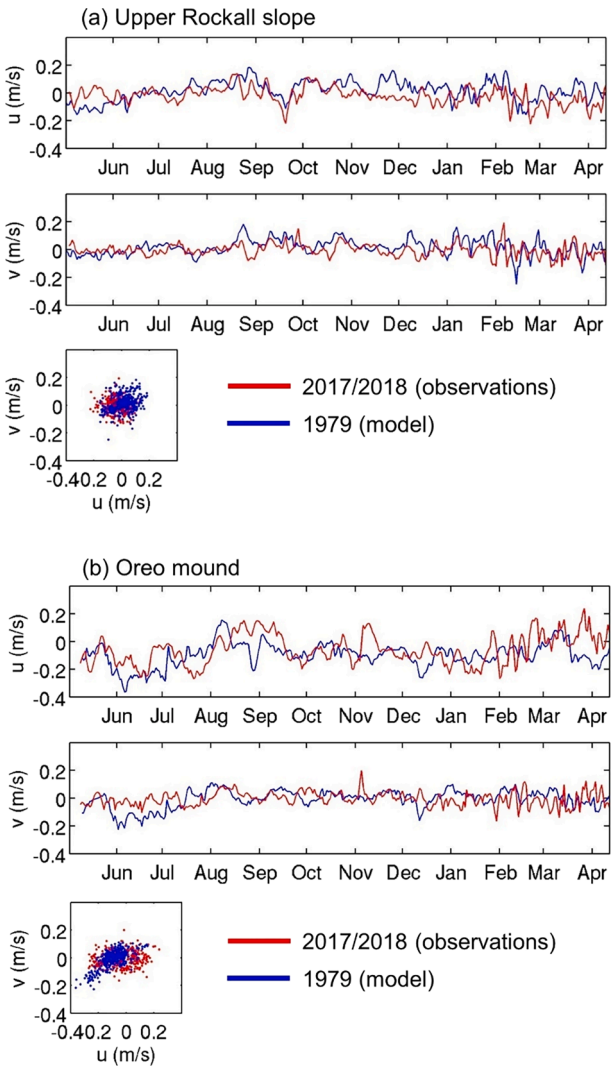

Fig. 4. 345-day time series of current velocities recorded by ADCPs from May 2017 to April 2018 at the upper Rockall Bank slope and at Oreo mound (red lines and scatter points; Schulz et al., 2020). Corresponding modelled current velocities (daily averaged output, 1979/1980 simulations) are displayed as blue lines and scatter points (see Table 2 for more information about mooring location and sampling period). (a) Upper Rockall Bank slope, (b) Oreo mound. Please note supplementary Fig. S2 for a more detailed analysis of current spectra.

(Fig. 4 a, b). At Oreo mound, however, the model results could not entirely reproduce the stronger variability in the observations during periods of frequent changes in magnitude and direction between January and April 2018 (Fig. 4 b). Despite the bias in time between model simulations and observations, the results of the performance statistics for individual velocity components and all available model-observation pairs suggest a good level of model agreement (Table 3). The analysis of current spectra from 3-hourly observed and modelled timeseries at both mooring locations sub-sampled in July 2017 (observations) and July 1979 (model) confirmed that strongly amplified diurnal tidal currents dominate the near-bottom tidal spectrum and its higher harmonics (supplementary Fig. S2). Even though we applied realistic boundary conditions and high vertical resolution close to the seafloor, the intrinsic variability and tidal dynamics resolved by our model does not include non-linear processes such as breaking internal waves and turbulent mixing at very small spatial scales. As a consequence, the model results likely underestimate realistic near-bottom velocity shear and kinetic energy dissipation rates. We accepted this

Table 3
Model performance statistics for all available model-observation pairs.

Location	Number of model-observation pairs (N)	CF (u velocity component)	CF (v velocity component
SE Rockall Bank (Logachev province), 10 m above bottom	353 (3-hourly)	1.54	1.38
SE Rockall Bank (Logachev province), 150 m above bottom	353 (3-hourly)	1.69	1.46
SE Rockall Bank (Oreo mound)	345 (daily)	0.93	1.24
SE Rockall Bank (upper slope)	345 (daily)	1.34	1.22

trade-off due to computational limitations and for the benefit of incorporating basin-scale variations in contrasting AMOC states and their propagation into the local CWC area models. Additional uncertainties in our model solutions could be due to the choice of COADS05 atmospheric forcing instead of data from multi-year simulations, such as CORE2. We accepted this limitation in our model approach because of the higher spatial resolution of COADS05 and our focus on evaluating AMOC states (represented by the VIKING20 lateral boundary conditions).

4.2. *Near-bottom water mass properties and currents*

At SE Rockall Bank, the highest modelled near-bottom θ and S values appear in the 600–1200 m depth range and over the larger carbonate mounds, but conditions differ considerably between periods of weak and strong AMOC (Fig. 5). In weak AMOC years (1978–1980) water in this depth corridor is warmer (1 °C) and saltier (0.15) than comparable θ and S characteristics in strong AMOC years (Fig. 5 e, f). The highest θ and S values are 9 °C and 35.5 in weak AMOC years (Fig. 5 a, b) and 8 °C and 35.35 during strong AMOC (Fig. 5 c, d).

Corresponding near bottom densities, expressed as potential density anomalies σ_θ (kg m^{-3}), vary between 27.5 kg m^{-3} along the upper slopes and 27.9 kg m^{-3} at water depths > 1800 m (Fig. 6). Modelled near-bottom densities within the SE Rockall Bank carbonate mound depth corridor (600–1200 m) are in the range 27.5–27.65 kg m^{-3} (Fig. 6 a, b). This density range agrees with the findings of previous studies reporting a characteristic density envelope of σ_θ = 27.35–27.65 kg m^{-3} for CWC presence in the Northeast Atlantic (e.g., Dullo et al., 2008). Near-bottom differences of potential density between AMOC states are generally small inside the depth range 600–1200 m ($\Delta\ \sigma_\theta < 0.04$ kg m^{-3}) as compared to the density envelope at which cold-water corals are found.

The near-bottom circulation is dominated by a southwestward along-slope current (Fig. 7). During strong AMOC, current magnitudes are intensified in the 600–1200 m depth range along the entire continental slope (Fig. 7 c, d), whereas during weak AMOC stronger currents are restricted to areas of abrupt topographic changes (Fig. 7 a, b). The highest current magnitudes during strong AMOC are 0.4 m s^{-1}, an increase of 0.1 m s^{-1} when compared to maximum values seen in weak AMOC years. A notable exception is Haas mound, a large carbonate mound structure, where changes in current velocities between different states of the AMOC are small above the summit and northeastern side, but strong along the southern side of the mound.

At Condor Seamount, water mass properties in the bottom-most layer over the summit and the upper slopes (<1000 m) are largely decoupled from conditions at greater depths. Temperature and salinity differences between periods of weak and strong AMOC at these shallower depths show an opposite trend when compared to conditions at SE Rockall Bank (Fig. 8). According to model predictions, waters in these upper layers are up to 1 °C warmer and 0.15 saltier in the early 1990s (strong AMOC) than in the late 1970s (weak AMOC). In contrast, θ and S differences in deeper waters at depths > 1000 m are much smaller. At intermediate depths (400–1000 m), mean θ and S values vary from 8.5 °C (weak

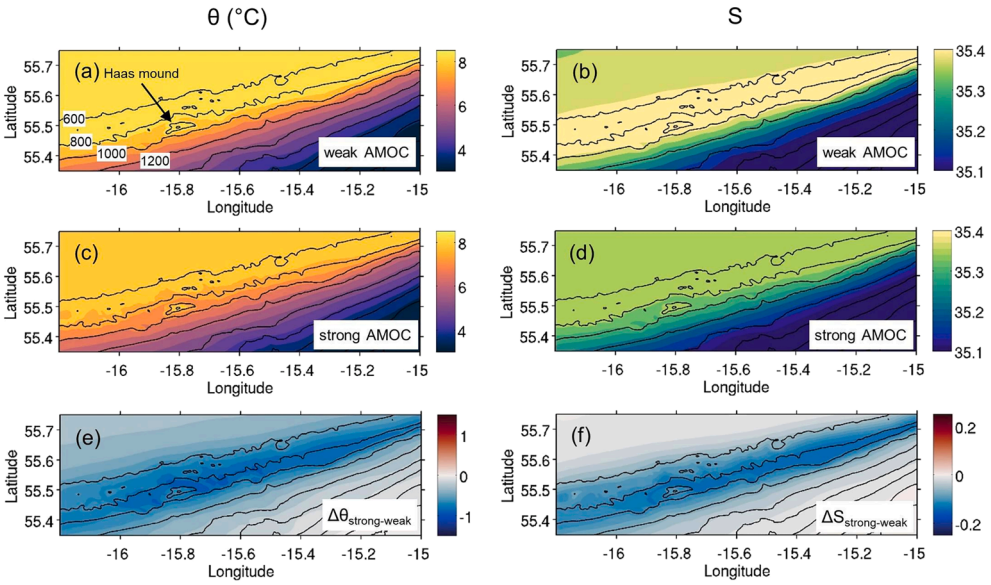

Fig. 5. Composites of potential temperature θ (°C) and salinity S in the bottom-most layer of the SE Rockall Bank model. (a, b) Weak AMOC years (1978–1980), (c, d) strong AMOC years (1992–1994), (e, f) difference between strong and weak AMOC state. The composites are time averaged over AMOC states from daily averaged model output. Depth contours in 200 m intervals between 600 m and 2400 m depth are superimposed. The horizontal resolution of the embedded model grid is 250 m.

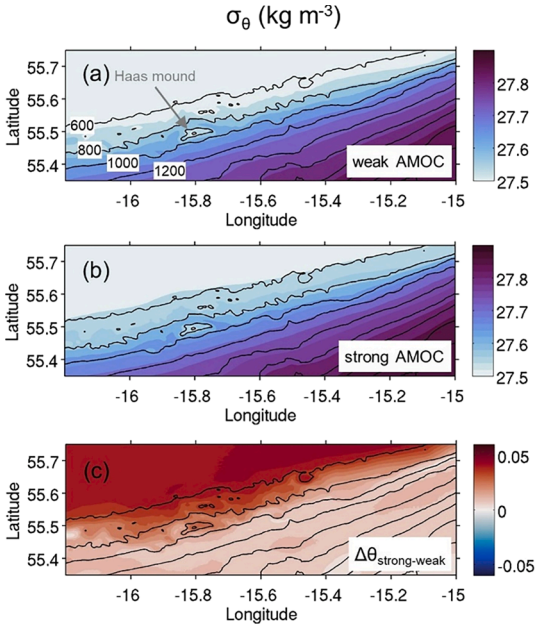

Fig. 6. Composites of potential density anomaly σ_θ (kg m^{-3}) in the bottom-most layer of the SE Rockall Bank model. (a) Weak AMOC years (1978–1980), (b) strong AMOC years (1992–1994), (c) difference between strong and weak AMOC state. The composites are time averaged over AMOC states from daily averaged model output. Depth contours in 200 m intervals between 600 m and 2400 m depth are superimposed. The horizontal resolution of the embedded model grid is 250 m.

AMOC years) to 9.5 °C (strong AMOC years) and 35.6 (weak AMOC years) to 35.75 (strong AMOC years) respectively. Over the central Condor seamount summit at depths ≤ 400 m, θ and S differences between AMOC states are considerably smaller, but θ and S are still elevated ($\Delta\theta = 0.5$ °C and $\Delta S = 0.05$) in periods of strong AMOC (Fig. 8 e, f).

The corresponding near-bottom potential densities over the summit are in the range $\sigma_\theta = 26.8$–27.2 kg m^{-3} increasing to $\sigma_\theta = 27.5$ kg m^{-3} in the deep waters surrounding the Condor seamount summit region (Fig. 9 a, b). Again in contrast to conditions at Rockall Bank, the model predictions show lower density anomalies in near-bottom layers in years of strong AMOC (Fig. 9 c).

The largest differences in current magnitude are ± 0.02 m s^{-1} between strong and weak AMOC years and can be found around the seamount at depths < 1000 m (Fig. 10 e). There is no consistent pattern which can be clearly assigned to a specific AMOC state, but overall, currents along the seamount rim seem enhanced in weak AMOC years (Fig. 10 e). The time-mean circulation at depths > 400 m is along-slope forming an anti-cyclonic vortex with maximum velocities of 0.05 m s^{-1} (Fig. 10 a–d). Atop the summit (<400 m) and at the deeper seamount flanks to the Northwest and Southeast, the mean flow is largely across isobaths and maximum velocities are up to 0.1 m s^{-1} (NW and SE edges) and 0.05 m s^{-1} (atop the summit; Fig. 10 a–d). Both flow magnitudes and directions are in good agreement with published (but not publicly available) current measurements conducted during the Condor observatory project 2009/2010 (Bashmachnikov et al., 2013). This study concluded that the vortex was stable over at least half a year during the observation period and mainly driven by tidal dynamics.

4.3. Seasonal variations

At SE Rockall Bank, seasonal variations of near-bottom, daily averaged currents during weak and strong AMOC years are comparable except for strongly enhanced currents (magnitudes up to 0.35 m s^{-1}) between January and the end of February during strong AMOC years (Fig. 11 e). Differences are smaller during the rest of the year with an increase in current magnitudes towards the summer and a decrease in autumn superimposed on a spring-neap tidal cycle during both AMOC periods (Fig. 11 e). Seasonal bottom temperature and salinity variations are in the range of 0.5–0.8 °C and up to 0.05 respectively (Fig. 11 a, c). In contrast, θ and S differences between weak and strong AMOC years can be twice as high showing persistently elevated values in weak AMOC years (Fig. 11 a, c). At Condor Seamount mean current magnitudes vary only slightly throughout the year between 0.05 m s^{-1} from January to July and 0.08 m s^{-1} from August to November modulated by the fortnightly spring-neap tidal cycle (Fig. 11 f). Differences in currents between weak and strong AMOC years are generally small with an almost identical seasonal evolution of magnitude and phase (Fig. 11 f). Both seasonal and inter-decadal variations in near bottom θ and S are less pronounced and reach only about half the magnitude of the changes at Rockall Bank (Fig. 11 b, d). A particularly notable feature is that θ and S distributions show an inverse relationship when compared to SE Rockall Bank with higher values during weak AMOC years.

Power spectra of instantaneous currents at two locations in the SE

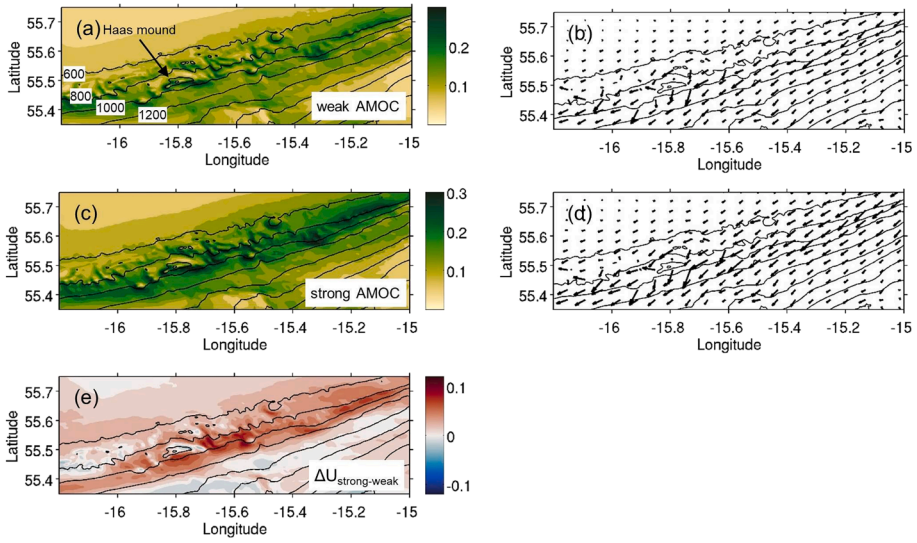

Fig. 7. Composites of currents in the bottom-most layer of the SE Rockall Bank model. (a) Current magnitude U (m s^{-1}) and (b) current vectors in weak AMOC years (1978–1980), (c, d) strong AMOC years (1992–1994), (e) difference of current magnitude between strong and weak AMOC state. The composites are time averaged over different AMOC states based on daily averaged model output. Depth contours in 200 m intervals between 600 m and 2400 m depth are superimposed. The horizontal resolution of the embedded model grid is 250 m.

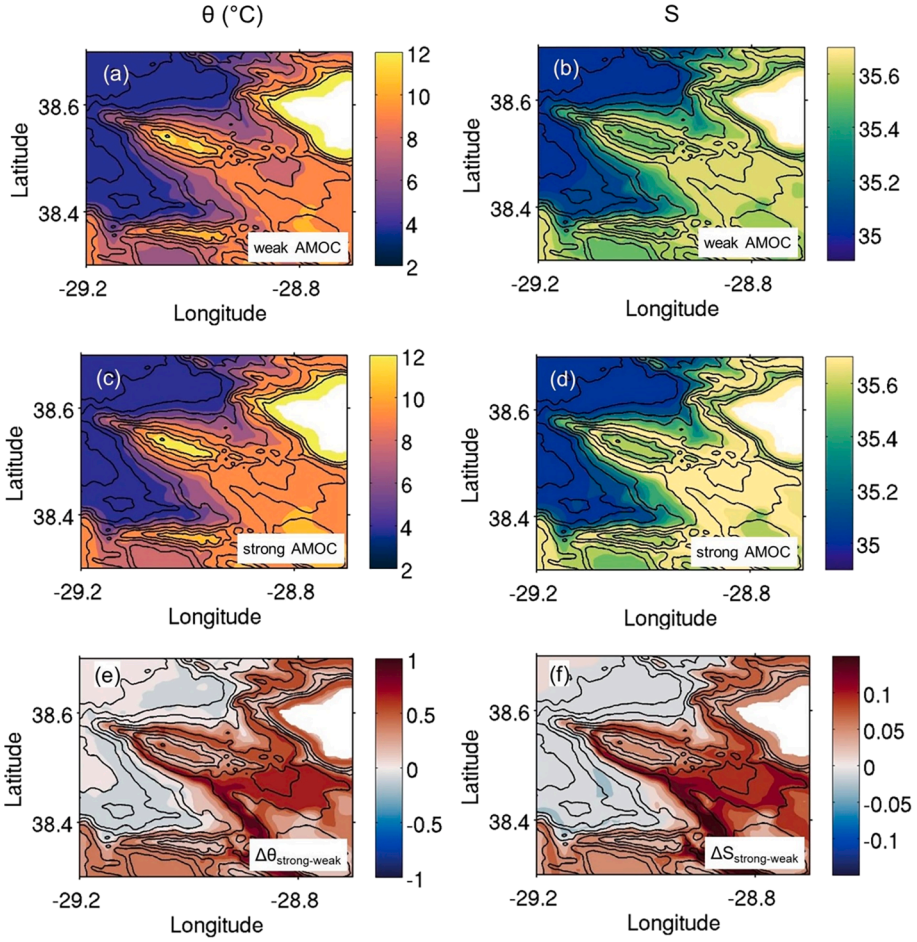

Fig. 8. Composites of potential temperature θ (°C) and salinity S in the bottom-most layer of the Condor Seamount model. (a, b) Weak AMOC years (1978–1980); (c, d) strong AMOC years (1992–1994); (e, f) difference between strong and weak AMOC states. The composites are time averaged over different AMOC states based on daily averaged model output. Depth contours in 200 m intervals between 200 m and 1800 m depth are superimposed (see Fig. 1 b for depth label numbering). The horizontal resolution of the embedded model grid is 250 m (only part of the model domain is shown).

Rockall Bank area (Oreo mound) and Condor Seamount (central summit) are presented in Fig. 12 to describe variations in the tidal spectrum. At SE Rockall Bank, the current spectra in the tidal frequency band show the clearest peaks at diurnal frequencies with additional peaks at less energetic semidiurnal frequencies and higher harmonics (Fig. 12 a, b). There is little variation between seasons and AMOC states in the diurnal frequencies (Fig. 12 a, b). At Condor Seamount, the most energetic tidal frequency currents are dominated by semi-diurnal oscillations that exhibit only small seasonal and inter-annual variations. At diurnal frequencies, however, the spectral peaks show considerably higher seasonal variability with generally enhanced spectral densities in summer during both AMOC states (Fig. 12 c, d). It should be noted that seasonal and AMOC related variations in tidal dynamics at these two locations have to be considered as snapshots largely controlled by local

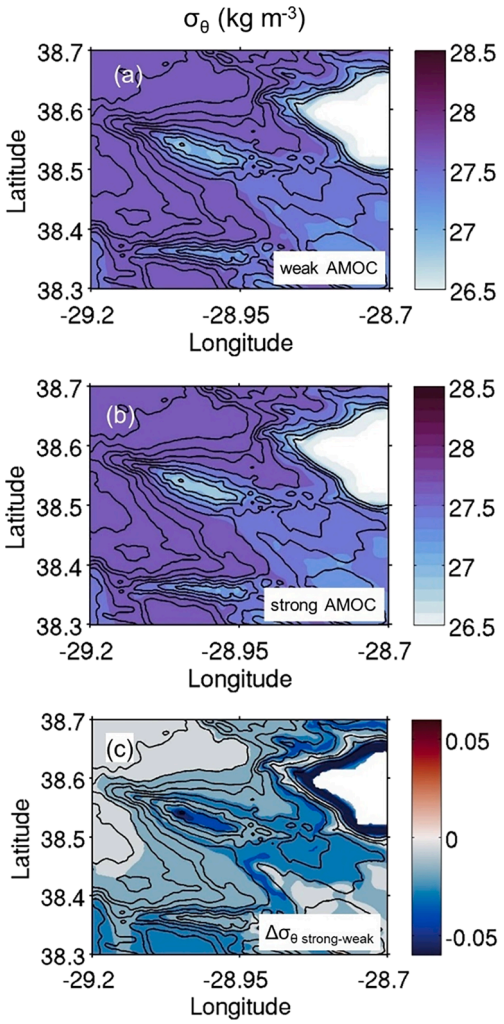

Fig. 9. Composites of potential density anomaly σ_θ (kg m^{-3}) in the bottom-most layer of the Condor Seamount model. (a) Weak AMOC years (1978–1980); (b) strong AMOC years (1992–1994); (c) difference between strong and weak AMOC states. The composites are time averaged over different AMOC states based on daily averaged model output. Depth contours in 200 m intervals between 200 m and 1800 m depth are superimposed (see Fig. 1 b for depth label numbering). The horizontal resolution of the embedded model grid is 250 m (only part of the model domain is shown).

stratification and bottom slope.

4.4. Local energy conversion and dissipation

Near-bottom distributions of rates of kinetic energy dissipation for both sites and AMOC states are presented in Fig. 13. At SE Rockall Bank, mean kinetic energy dissipation is enhanced in the strong AMOC state above the large carbonate mounds of the Logachev province in the 600 m–1000 m depth range. Kinetic energy dissipation in these regions is up to two orders of magnitudes higher than the largest dissipation rates outside this depth corridor in the shallower and deeper parts of the SE Rockall Bank slope (Fig. 13 a, c). Kinetic energy dissipation rates are generally enhanced during strong AMOC, but do not always show a consistent pattern upstream and downstream of the larger coral mounds (Fig. 13 e). At Condor Seamount, near-bottom kinetic energy dissipation is highest along the major axis of the seamount with maximum rates above the summit regions (bottom depths $<$ 400 m) and along the deeper parts of the northwestern and southeastern slopes (Fig. 13 b, d). Kinetic energy dissipation rates at Condor Seamount are generally much smaller than the high near-bottom kinetic energy dissipation rates predicted above the large carbonate mounds at SE Rockall Bank. Consistent with the results from SE Rockall Bank, differences between AMOC periods in the near-bottom layers are small (Fig. 13 f).

Vertical distributions of mean kinetic energy dissipation rates along two cross-slope transects at the SE Rockall Bank slope and along a N-S transect across the central part of Condor Seamount summit are shown in Fig. 14. Kinetic energy dissipation rates in all areas are surface intensified in the upper 50 m driven by seasonal and shorter-period changes of the near-surface circulation due to variations in the wind field, passing sub-mesoscale fronts and eddies and the annual warming and cooling cycle. In the deeper ocean, kinetic energy dissipation rates are enhanced above rough topography dominated by tide-topography interaction. High rates of kinetic energy dissipation above Haas mound (the largest carbonate mound along the SE Rockall Bank) extend $>$300 m into the water column with larger excursions during strong AMOC (Fig. 14 a, b, c). Thus, interior ocean mixing is potentially intensified in periods of both weak and strong AMOC. This strong coupling of surface and near-bottom kinetic energy dissipation rates is less intense in regions of shallower slopes, but still amplified in strong AMOC years (Fig. 14 d, e, f). At Condor Seamount, maximum rates of kinetic energy dissipation are limited to water depths shallower than 400 m indicating local amplification of tide generated seamount trapped waves inside a stable Taylor Cap as the main contributing mechanism (Bashmachnikov et al., 2013). Kinetic energy dissipation rates drop to lower levels on the deeper seamount flanks below 500 m depth. There is little difference in kinetic energy dissipation rates between periods of weak and strong AMOC indicating that near-bottom dynamics at summit level and above is largely dominated by tide-topography interactions (Fig. 14 g, h, i).

5. Discussion

5.1. AMOC variability, local response and ecological implications

In this study, we aimed to investigate the relative influence of tidal to multi-decadal, basin-scale variability on near-bottom hydrodynamics at two contrasting regions hosting rich and diverse cold-water coral communities. At SE Rockall Bank, large coral assemblages of the genus *Desmophyllum* exist in a narrow depth corridor (600–1200 m; Kenyon et al., 2003) matching the depth range of the strongest near-bottom currents observed above and around large carbonate mounds (White and Dorschel, 2010). Oceanic motions at SE Rockall Bank exist along a broad spectrum of frequencies and magnitudes and include along-slope residual currents, bottom-trapped diurnal waves amplified to magnitudes of 0.45 m s^{-1}, breaking internal waves and turbulent mixing (Mienis et al., 2007; Cyr et al., 2016; van Haren et al., 2014; Schulz et al., 2020). The Rockall Trough including Rockall Bank is an area of deep-reaching winter convection down to depths of 500–700 m (Penny Holliday et al., 2000), which marks the upper boundary of dense CWC aggregations and carbonate mounds in the region. Convection is most intense during the winter-spring transition descending into the permanent thermocline promoting strongly enhanced residual currents and baroclinic waves (White and Dorschel, 2010). These conditions of intensified currents involve high turbidity levels in bottom waters (suggesting sediment resuspension) and lead to enhanced organic matter and sediment fluxes both along and across slope, favoring food supply and mound growth (Mienis et al., 2009; Soetaert et al., 2016; Schulz et al., 2020).

In our model simulations, AMOC related changes of bottom-water temperature and salinity in the CWC corridor at 600–1200 m depth (while less sensitive to CWC distribution) are marked by significant cooling and freshening during strong AMOC years (parameters θ and S in Fig. 15 a, b). In the North Atlantic, thriving CWC reefs have been linked to well defined physical and hydrochemical boundaries inside a narrow density envelope of potential density σ_θ = 27.35–27.65 kg m^{-3} (Dullo et al., 2008; Flögel et al., 2014). Our model results in CWC presence

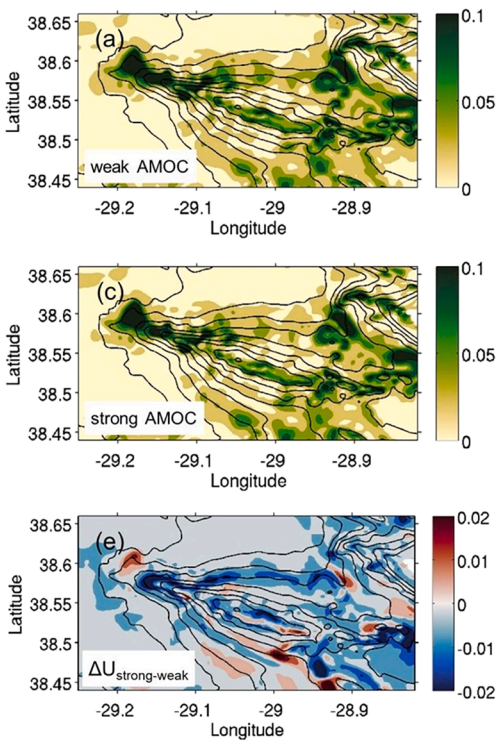

Fig. 10. Composites of currents in the bottom-most layer of the Condor Seamount model. Current magnitude U (m s^{-1}) and current vectors in (a, b) weak AMOC years (1978–1980) and (c, d) strong AMOC years (1992–1994), respectively and (e) difference in current magnitude between strong and weak AMOC state. The composites are time averaged over different AMOC states based on daily averaged model output. Depth contours in 200 m intervals between 200 m and 1800 m depth are superimposed (see Fig. 1 b for depth label numbering). The horizontal resolution of the embedded model grid is 250 m (only part of the model domain is shown with a focus on the central Condor Seamount area).

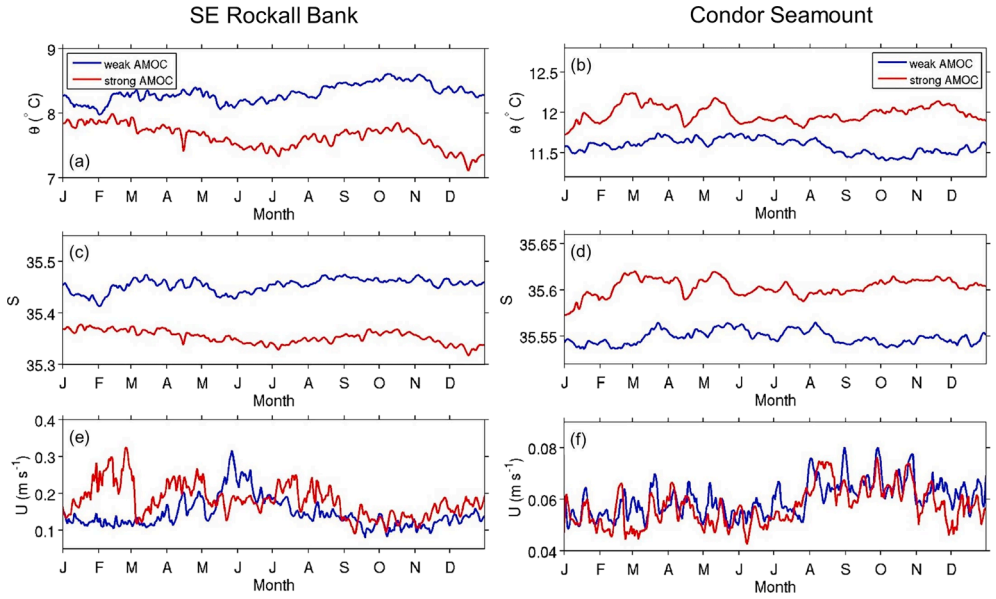

Fig. 11. Time series (daily averages) of near-bottom distributions of potential temperature θ (°C), salinity S and, current magnitude U (m s^{-1}) at SE Rockall Bank (a, c, e) and Condor Seamount (b, d, f). The time series represent an annual climatology calculated from model data averaged over each respective AMOC period at bottom depths 600 m < H < 1200 m (SE Rockall Bank) and H ≤ 400 m (Condor seamount).

locations fall well within this proposed density envelope with only small variations between AMOC states (parameter σ_θ in Fig. 15 a). Bottom current magnitudes were generally enhanced at predicted CWC presence locations and during periods of strong AMOC in comparison with corresponding pseudo absence locations and weak AMOC state (U in Fig. 15 a, b). In contrast, differences in kinetic energy dissipation rates between periods of weak and strong AMOC are much smaller at CWC presence locations (parameter ε in Fig. 15 a), but magnitudes are almost one order of magnitude higher than in modelled CWC pseudo absence locations (parameter ε in Fig. 15 b).

These predicted changes in near-bottom water mass properties and currents agree well with previously reported principal patterns of basin-scale and regional-scale ocean climate variations in the subpolar NE Atlantic. For example, the northeastward SPG expansion in a strong AMOC state contributed to intensified currents and lower salinities in the upper and bottom waters of the Rockall-Hatton Plateau and corresponded to enhanced biological production (Hátún et al., 2009b, 2016; Johnson et al., 2020). Notable periods of higher salinity in upper ocean waters (<600 m) were observed in the Northern Rockall Trough between 1980 and 1986 and after 1995 (Holliday et al., 2015). Bottom

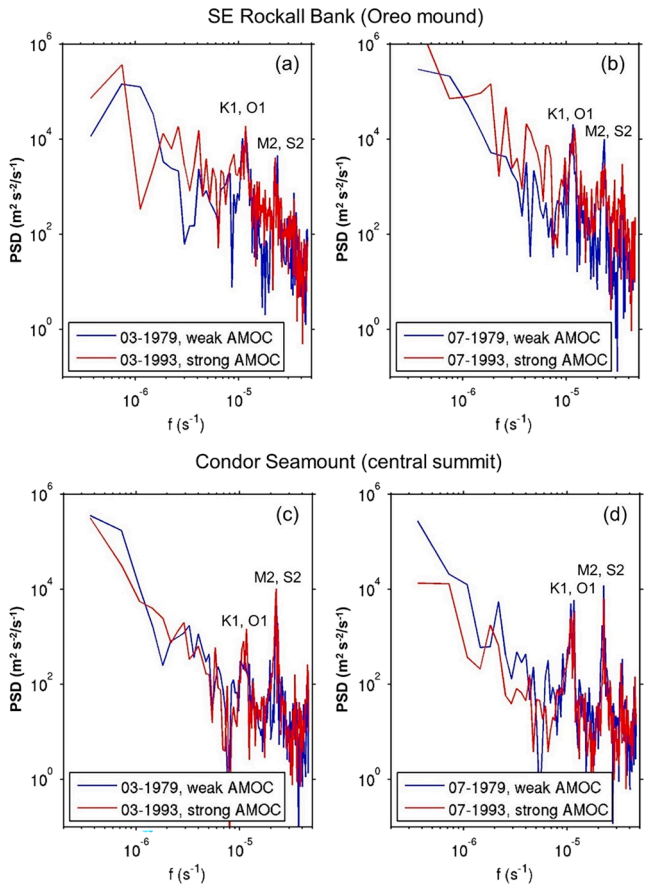

Fig. 12. Power spectra calculated from 3-hourly modelled near-bottom currents (31 days) at two locations in the SE Rockall Bank and Condor Seamount area. The locations are indicated in Fig. 1. The time series represent conditions in spring (March, a and c) and summer (July, b and d) during periods of weak (1979) and strong (1993) AMOC. The x-axis displays the frequency f (s^{-1}) and the y-axis displays the power spectral density scaled by the frequency f (m^2 s^{-2}/s^{-1}).

kinetic energy differences between weak and strong AMOC periods (Fig. 16) show a clear increase in bottom kinetic energy during strong AMOC associated with overflow regions (Faroe Bank Channel overflow, Denmark Strait overflow) and boundary currents (Irminger Current south of Greenland, Shelf Edge Current poleward along the eastern Rockall Trough). Bottom kinetic energy is also enhanced around the Wyville Thomson Ridge and the NW Rockall Trough stretching out over the Rockall-Hatton Bank as a narrow belt confined to a depth range of 1000 m–2000 m (Fig. 16).

Shifts in the future ocean climate beyond the largest present day AMOC displacements might move environmental extremes towards critical tipping points, likely impeding deep-sea benthic species to adapt to the new environmental conditions, even though benthic fauna (and CWCs in particular) is occasionally exposed to large changes in their physical environment (Mienis et al., 2014). Adverse effects of long-term climate change in the deep-sea will degrade biodiversity through a reduction of organic matter flux because of an intensified stratification, which could eventually block nutrient supply to surface layers in a warmer upper ocean (Sweetman et al., 2017). Predicted distributions of suitable CWC habitats in a future ocean exposed to high levels of emissions indicate a substantial decline of the areas occupied by coral species, limiting the sites that could be considered climate refugia by 2100 (Morato et al., 2020). Even on shorter time scales, interannual changes in bottom temperature, bottom salinity and NAO (North Atlantic Oscillation) rather than seabed morphology were found to explain variations in macrofaunal communities in the Mingulay CWC reef in the NE Atlantic (Kazanidis et al, 2021). There, differences in community composition and diversity were attributed to interannual variability in bottom temperature, whereas no or only small differences were observed in species richness (Kazanidis et al., 2021). Thus, understanding ecological tipping point crossings requires consideration of multiple factors, spatial and temporal scales, as well as integration of different disciplines (Hebbeln et al., 2019). Such a multi-factor approach could not only involve the assessment of functional relationships between CWC ecosystem components and changes in physical and hydrochemical water properties over space and time but should also consider the role of physical processes and mechanisms that drive food supply.

At Condor Seamount, our model results indicate little variation of near-bottom dynamics in response to basin-scale changes of the AMOC. The combination of energetic internal tides and associated local mixing has the potential to retain an important, high quality food supply for suspension feeders atop the Condor summit and along the upper seamount flanks. This is in line with results of Rovelli et al. (2022), who suggested that the residence times of water (and thus suspended matter) within benthic communities at the seamount summit plays an important role for maintaining coral gardens. Flow velocities within the gardens were found to be significantly lower (i.e., longer residence times) than sandy reference sites, both within the summit area and just 10 s of meters off the coral gardens.

Reefs and other CWC habitats (such as coral gardens) have been recognized as hotspots for carbon cycling (van Oevelen et al., 2009; White et al., 2012; Rovelli et al., 2015, 2022; Cathalot et al., 2015; de Froe et al., 2019; De Clippele et al., 2021). The enhanced supply and turnover of organic carbon in these communities result from an interplay and coupling between the community's ability to draw down available food from the water column and the physical processes that focus and replenish food supplies to CWC habitats. Biophysical coupling at shallow seamounts has often been discussed in the context of tracer retention inside stable Taylor caps accompanied by enhanced primary and secondary production (e.g., White et al., 2008). However, effects of seamount flow dynamics on biological distribution patterns takes many forms. These include retention and loss of plankton, resuspension of sediments by enhanced turbulent mixing and current shear in the seamount bottom boundary layer, which support food supply to suspension feeders like corals and filter feeding sponges (Genin, 2004; Genin and Dower, 2007; Mohn et al., 2021). The general assumption of enhanced and persistent aggregation of biological material over seamount summits, however, is not often supported by observations and strongly varies between seamounts (e.g., McClain, 2007).

At Condor seamount, Bashmachnikov et al. (2013) largely excluded the potential for enhanced primary production over the summit, as the Taylor cap was confined to depths below 170 m, well under the euphotic zone and the seasonal thermocline. Santos et al. (2013) confirmed this assertion as they could not find evidence of increased phytoplankton concentrations at depths < 100 m above Condor seamount. In contrast, there was clear evidence of strong acoustic backscatter over the summits of Condor seamount, which could be attributed to the presence and retention of resident micronekton (Cascão et al., 2017). These are not necessarily contradicting findings – previous results have highlighted the importance of swimming micronekton for maintaining seamount-associated population distributions (e.g., Wilson and Boehlert, 2004). The episodic shedding and restoration of Taylor caps reported at Condor seamount may support trophic enrichment over the seamount by subsidy of planktonic material through horizontal advection from the far field towards the seamount (Genin and Dower, 2007).

However, multi-decadal changes in sea-surface temperature, chl-a and net primary productivity (NPP) in the Azores region showed a clear warming trend, combined with negative trends in chl-a and NPP over the past 40 years (Signorini et al., 2015; Siemer et al., 2021). Analysis of the surface geostrophic velocity from EN4 monthly data in the oceanic far field surrounding Condor Seamount since 1990 indicates

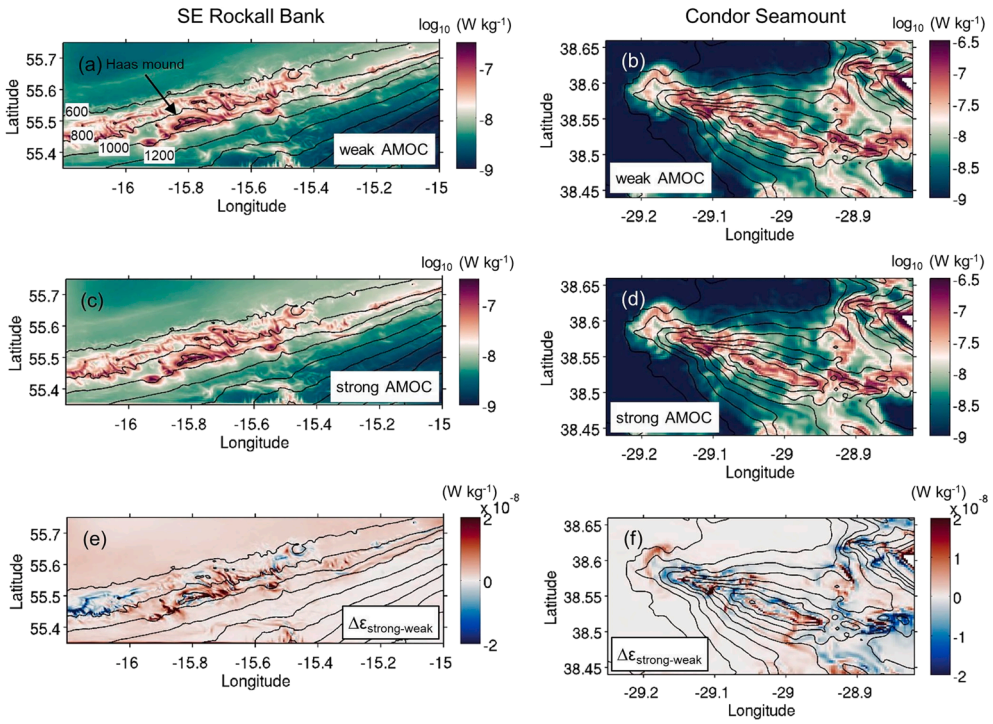

Fig. 13. Mean near-bottom kinetic energy dissipation rate $\log_{10}(\varepsilon)$ (W kg^{-1}) for weak (a, b) and strong (c, d) AMOC years in the bottom-most layer of SE Rockall Bank and Condor Seamount, respectively, calculated from daily averaged model output of the 3D current velocity field. Differences in ε between weak and strong AMOC years (e, f) are not log transformed and in units W kg^{-1}. Depth contours in 200 m intervals between 200 m and 2400 m depth are superimposed. The horizontal resolution of the model grid is 250 m. At Condor Seamount, only part of the model domain is shown with a focus on the central seamount area.

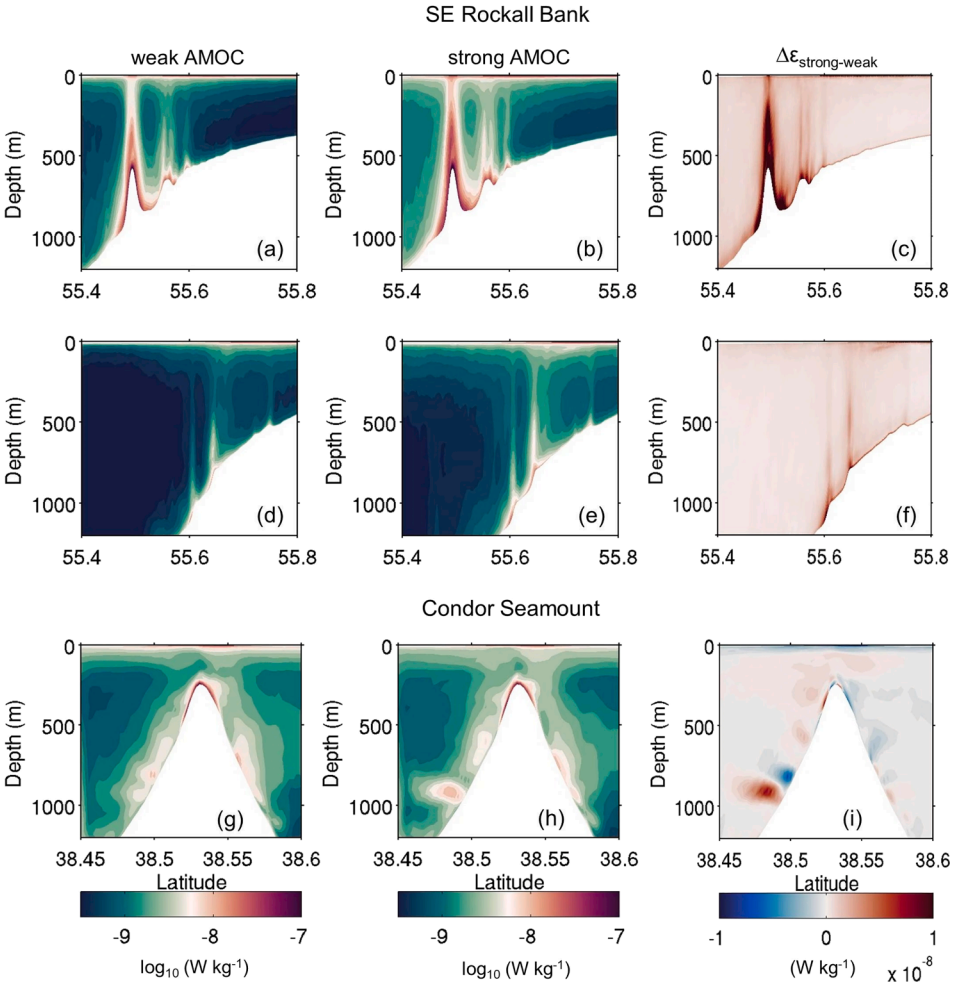

Fig. 14. Mean kinetic energy dissipation rate $\log_{10}$ (ε) (W kg^{-1}) for different AMOC periods along cross-slope (North-South) transects. (a, b, c) SE Rockall Bank (Haas mound, longitude 15.808 °W); (d, e, f) SE Rockall Bank (longitude 15.25 °W); (g, h, i) Condor Seamount (longitude 29.027 °W). The analysis is based on daily averaged model output of the 3D velocity field. The horizontal resolution of each embedded model grid is 250 m. The regions are not equally scaled due to their different size. (c, f, i) are not log transformed and in units W kg^{-1}. Subplots (c, f, i) represent the difference between strong AMOC and weak AMOC.

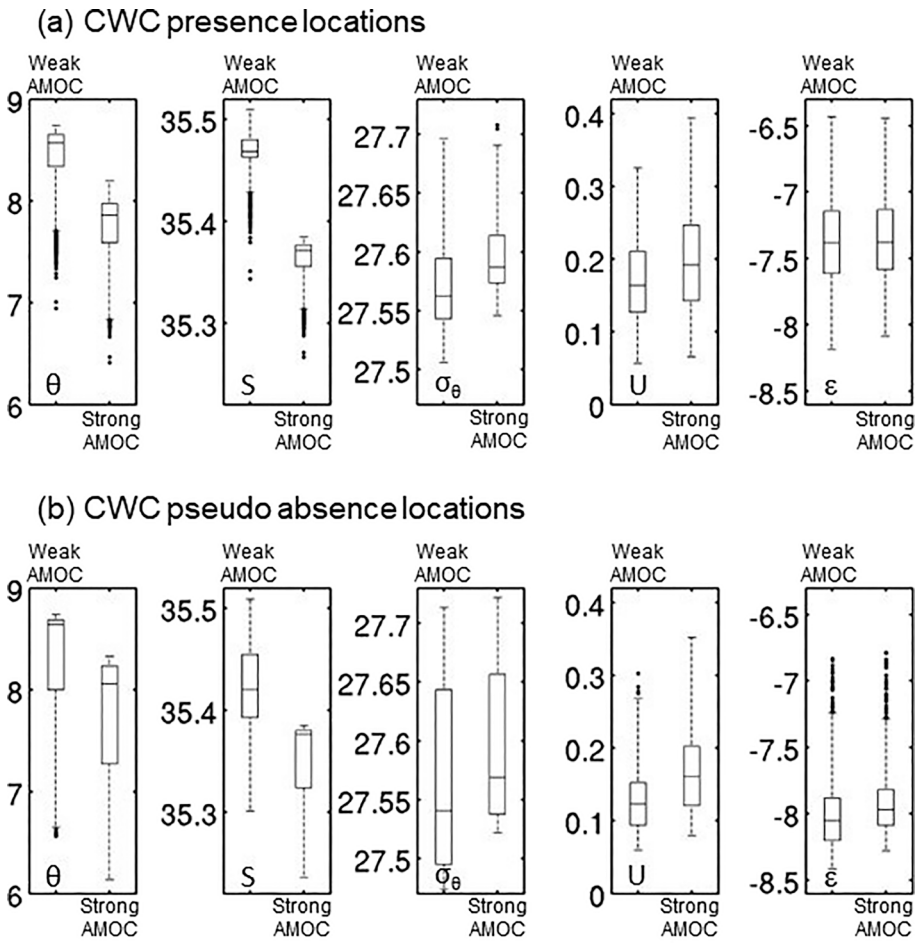

Fig. 15. Box plots of near-bottom temperature θ (°C), salinity S, potential density σ_θ (kg m^{-3}), current magnitude U (m s^{-1}) and kinetic energy dissipation $\log_{10}$ (ε) (W kg^{-1}) at (a) CWC presence and (b) randomly selected (pseudo) absence locations at SE Rockall Bank during periods of weak and strong AMOC. Black bars in the center represent the median. Black boxes represent the 25 and 75 % quartiles. Whiskers extend two times the interquartile range indicating the spreading of values from minimum to maximum across the interquartile. CWC presence data were extracted from the habitat suitability model by Rengstorf et al. (2014) and Soetaert et al. (2016). Random absence locations were extracted in the depth range 600–1200 m.

that the observed warming trend is accompanied by a continuous weakening of the southward surface flow in the vicinity of the seamount (Fig. 17). This weaker surface flow will reduce the flux of organic matter to the seamount in a future scenario of a warmer North Atlantic as a consequence of reduced advection and enhanced stratification.

5.2. *Kinetic energy dissipation as a mechanistic proxy for species distribution*

Due to their structural complexity, fragility, and critical exposure to various potentially adverse anthropogenic impacts (fisheries, climate change), CWCs and sponges are considered indicators of vulnerable marine ecosystems (VMEs) with a high conservation value. Yet, we still only have scattered knowledge about their global distribution (Roberts and Cairns, 2014). Species distribution models (SDMs) are increasingly used to improve our often sparse knowledge of the distribution of VME indicator species, for which fragmented data on their ecology, environmental preferences and tolerances is generally available. Complex interactions of multiple environmental variables must be accurately evaluated as each variable may have opposite effects on species occurrence (Wienberg and Titschack, 2017). SDMs employ different methods to predict species distributions based on relationships between environmental predictor variables and species presence locations, usually involving machine learning algorithms (Davies and Guinotte, 2011; Chu et al., 2019; Sundahl et al., 2020, de Clippele et al., 2021, Morato et al., 2020). Still rather few species distribution modelling studies, however, include near-bottom currents in their collection of suitable predictor variables.

Local and persistent hydrodynamic hotspots and high advection rates of suspended organic material therefore seem prerequisite for the build-up and structuring of deep-sea scleractinan reefs, such as those made by *D. pertusum* (Roberts et al., 2006; White et al., 2007; White and Dorschel, 2010). The most frequently proposed mechanism behind the formation of such hotspots in the deep sea is the conversion of kinetic energy from large-scale currents and barotropic tides to internal tides and enhanced turbulence over rough topography (Nikurashin and Legg, 2011; Nikurashin et al., 2013). Frederiksen et al. (1992) found that the depth distribution of CWCs coincided with the zone where internal waves break and hypothesized that this phenomenon created local hydrodynamic hotspots. Since then, model studies have indicated that internal waves are in fact an important source for locally enhanced currents and vertical mixing at coral sites (Mohn et al., 2014; Soetaert et al., 2016; van der Kaaden et al., 2021) and this has been confirmed by observations across different spatial and temporal scales (Davies et al., 2009, Osterloff et al. 2019; Wienberg et al., 2020; De Froe et al., 2022). Typically, hydrodynamics in SDMs is represented as a depth-related function of current speed and current direction, used as proxy variables for sediment flux and food supply (Rengstorf et al., 2014; Sundahl et al., 2020). Our capacity to understand and predict the distribution of VME indicator species and their functioning at increasingly small management scales (<1 km), however, might require a more mechanistic and functional representation of hydrodynamics in SDMs. In this regard, SDMs should acknowledge internal wave dynamics, 3D velocity shear and dissipation of kinetic energy over rough terrain as important drivers of turbulent mixing and the supply of organic matter. This knowledge is increasingly delivered by predictions from mechanistic models (like those presented in this study) as well as cutting-edge in-situ sampling. For example, from high resolution temperature and current measurements at SE Rockall Bank, van Haren et al. (2014) concluded that turbulent mixing generated by breaking internal waves is more

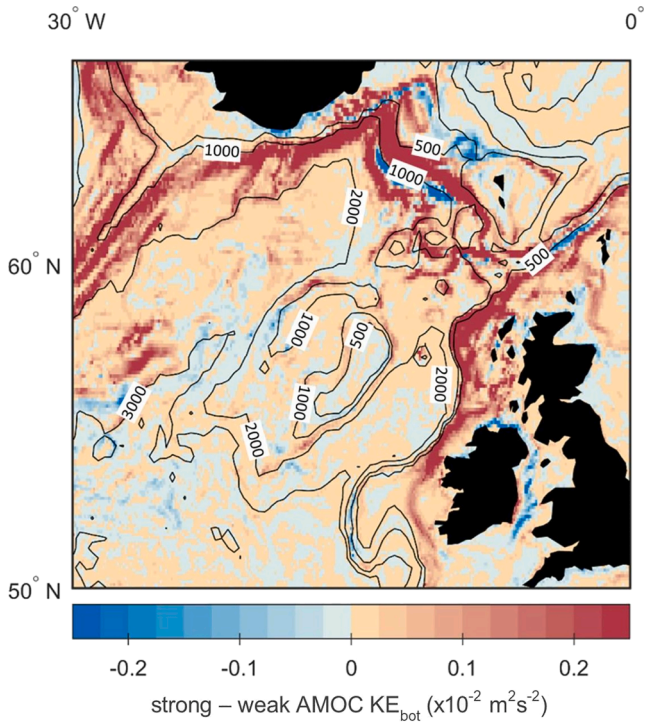

Fig. 16. Bottom kinetic energy differences between strong and weak AMOC periods based on output from the basin-scale VIKING20 model. Strong (weak) AMOC periods are defined as those above (below) one standard deviation from the mean. See Johnson et al. (2020) for methodology.

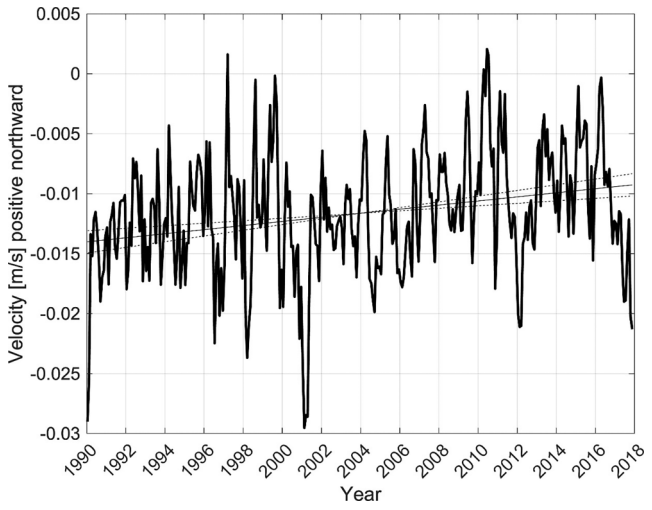

Fig. 17. Geostrophic velocity between CTD stations at 45°W and 15°W at a latitude of 37°N based on monthly EN4 data (Good et al., 2013). The velocity is computed relative to a zero velocity at 2500 m depth. The black line shows the linear fit with the 95 % confidence limits plotted as dashed black lines.

relevant for understanding CWC growth than current magnitude. Our model results indicate that locations of enhanced kinetic energy dissipation rates correspond well with modelled distributions of CWC habitat at SE Rockall Bank (Fig. 18). At Condor Seamount, the dip in kinetic energy dissipation from summit to slope also marks the boundary between an observed deep sponge belt around Condor at depths > 500 m and the dense coral gardens of the summit region (Tempera et al., 2012). This strong correlation between CWC distribution and enhanced kinetic energy dissipation suggests that there is a strong dependence of CWC distribution to an efficient and stable food supply mechanism and that

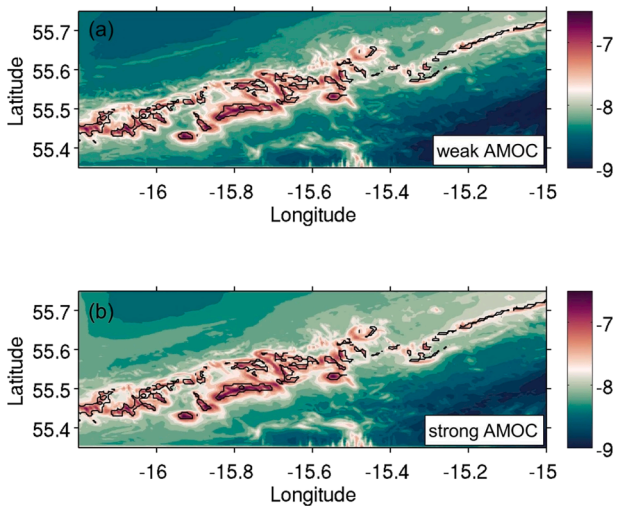

Fig. 18. Modelled distribution of near-bottom kinetic energy dissipation $\log_{10}(\varepsilon)$ (W kg^{-1}) at SE Rockall Bank (colored contours) during weak (a) and strong (b) AMOC years superimposed on predicted CWC occurrences (areas inside black lines) from the habitat suitability model by Rengstorf et al. (2014).

kinetic energy dissipation may therefore be a useful proxy for food supply. It also highlights the benefit of high-resolution hydrodynamic models in combination with detailed terrain data to resolve the 3-D velocity field at spatial scales that are relevant for the filtering efficiency of CWC reefs and larger sponge assemblages.

Flume experiments investigating the feeding habits of coral branches that include framework-building stony coral *D. pertusum* (Purser et al., 2010; Orejas et al., 2016), garden-forming octocorals *Dentomuricea* aff. *meteor* and *Viminella flagellum* (Rakka et al., 2021) and colony-building black coral *Antipathella wollastoni* (Rakka et al., 2020) have all indicated that feeding efficiency tends to be the highest under relatively low flow velocities (<7 cm s^{-1}). Moreover, the type of food source also plays an important role on feeding strategies. For example, *D. pertusum* might capture predominantly zooplankton at low flow velocities (2 cm s^{-1}) and phytoplankton at slightly higher flow velocities (5 cm s^{-1}), possibly allowing the corals to more efficiently exploit diverse food supply mechanisms, such as tidal driven and advective pathways (e.g., Orejas et al., 2016).

Preference of CWCs for intermediate current speeds is in interesting contrast with the numerous reports of CWC reefs occurring in areas with very strong bottom currents (Khripounoff et al., 2014; Roberts et al., 2009; White et al., 2007) or very low bottom currents (Lim et al., 2020). Non-invasive flow measurements at coral heights via the aquatic eddy covariance technique have shown that CWC assemblages mostly experience mean flows below 15 cm s^{-1} and down to 2–5 cm s^{-1}, in line with corals' optimal feeding efficiency (Rovelli et al., 2015, 2022). CWC framework also causes reduced bottom current speeds in its wake field (Mienis et al., 2019). Due to the structural and topographical complexity of CWC habitats, however, it remains challenging to generalize such findings. At Rockall Bank, coral-height mean flow velocities on top of Oreo mound were in excess of 80 cm s^{-1}, yet the mound thrived with dense assemblages of live CWC patches, while on the summit of the nearby Haas mound, CWCs showed a patchy distribution (de Froe et al., 2019; Maier et al., 2021), despite flow velocities were within the presumed optimal coral feeding range. CWC framework reducing bottom current speeds in its wake field could cause this patchy distribution (Mienis et al. 2019). Overall, our findings suggest that bottom kinetic energy dissipation might be a more suitable proxy for CWC biomass than bottom current speed, even if the modelled energy dissipation rates cannot be compared to realistic values due to the lack of measurements or other realistic studies from these areas.

6. Conclusions

In our study, we investigated the influence of AMOC related basin-scale changes in water mass properties and currents propagating into local-scale CWC and sponge areas dominated by tidal dynamics based on results from high-resolution model simulations. Our findings indicate different feedback of contrasting AMOC states in near-bottom waters of SE Rockall Bank and Condor Seamount. At SE Rockall Bank, basin-scale variations generate intensified bottom currents and kinetic energy dissipation bathing coral reef communities in cooler and less saline waters during periods of strong AMOC. At Condor Seamount, however, bottom currents appear largely unaffected by contrasting AMOC states at summit depths < 400 m, where the largest aggregations of coral gardens formed by the octocorals *Viminella flagellum* and *Dentomuricea* aff. *meteor* are observed. This study also highlights the need of incorporating processes driven by small-scale tide-topography interactions in species distribution modelling. In recent climate projections from SDMs, changes in small-scale hydrodynamics are not yet included. Oscillating flows along the spectrum from internal to fortnightly tides episodically intensified over steep topographic features would likely amplify AMOC induced changes in bottom currents and potentially further reduce suitable coral and sponge habitat. Accurate climate model data can narrow data gaps and improve both local high-resolution model hindcasts and future projections. To further investigate such complex interactions of live corals and coral framework with their turbulent environment at the coral patch scale, hydrodynamic models can be useful tools. It would be desirable that such models are capable to resolve the non-linear spectrum of physical processes including breaking internal waves and turbulent mixing at meter scales. Kinetic energy dissipation derived from our modelled 3D near-bottom velocity field appeared to relate closely with observed CWC locations. Hence, even though our model does not explicitly include non-linear dynamics such as turbulence and internal wave breaking, enhanced kinetic energy dissipation rates from our model may serve as a useful proxy to identify areas where kinetic energy transfer from lower to higher frequencies and non-linear motions may occur and thus may provide a dynamical link to coral ecology. This parameter is therefore proposed as part of a new class of functional descriptors of CWC distribution as it provides a more mechanistic view of hydrodynamics driving organic matter supply to filter and suspension-feeding communities.

Research data

The data set for set up, initial and boundary conditions of the high-resolution local area model implementations in two case study areas, Rockall Bank and Condor Seamount, are available online at zenodo (https://doi.org/10.5281/zenodo.3582932; Mohn et al., 2019). The data include the computational grids, initialization fields (temperature, salinity) and boundary conditions (temperature, salinity, currents, sea surface height) for the ROMS-AGRIF simulations presented in this study. EN.4.2.1 data with the g10 bias corrections were obtained from https://www.metoffice.gov.uk/hadobs/en4/ and are © Crown Copyright, Met Office, provided under a Non-Commercial Government Licence https://www.nationalarchives.gov.uk/doc/non-commercial-government-licence/version/2/.

Funding

This study has received funding from the European Union's Horizon 2020 Research and Innovation Programme under grant agreement nos. 678760 (ATLAS) and 818123 (iAtlantic). The output of this study reflects only the author's view, and the European Union cannot be held responsible for any use that may be made of the information contained therein. We acknowledge funding of the Netherlands Organisation for Scientific Research NWO and Royal Netherlands Institute for Sea Research NIOZ in organising the Netherlands Initiative Changing Oceans NICO expedition in 2018. This research was partially funded by the Netherlands Organisation for Scientific Research (VIDI grant 864.13.007). T.M. and M.C.S. were supported by the FCT-IP Stimulus of Scientific Employment Program (CCCIND/03345/2020 and CCCIND/03346/2020, respectively). C.D.-C. was supported by the FCT-IP Project UIDP/05634/2020. M.C.S., C.D.-C. and T.M. also acknowledge funds through the FCT – Foundation for Science and Technology, I.P. under the project OKEANOS UIDB/05634/2020 and UIDP/05634/2020 and through the FCT Regional Government of the Azores under the project M1.1.A/REEQ.CIENTÍFICO UI&D/2021/010.

Declaration of Competing Interest

The authors declare that they have no known competing financial interests or personal relationships that could have appeared to influence the work reported in this paper.

Data availability

I have shared the link to my research data in the manuscript in the section 'Research data'.

Acknowledgements

We thank Dr. Martin White (NUIG, Ireland) for providing time series of observed currents for model validation at SE Rockall Bank. We would also like to thank Dr. Erik Behrens (NIWA, New Zealand) and Prof. Arne Biastoch (GEOMAR, Germany) for providing us with an original unedited version of supplementary Fig. S4c (a) in Böning et al. (2016). We used cmocean colormaps for displaying oceanographic data in the manuscript (Thyng et al., 2016).The authors would like to acknowledge with great appreciation the very helpful and constructive comments from two anonymous reviewers.

Appendix A. Supplementary material

Supplementary data to this article can be found online at https://doi.org/10.1016/j.pocean.2023.103031.

References

Barbosa Aguiar, A.C., Peliz, A.J., Cordeiro Pires, A., Le Cann, B., 2011. Zonal structure of the mean flow and eddies in the Azores Current system. J. Geophys. Res. 116, C02012. https://doi.org/10.1029/2010JC006538.

Bashmachnikov, I., Mohn, C., Pelegrí, J.L., Martins, A., Jose, F., Machín, F., White, M., 2009. Interaction of Mediterranean water eddies with Sedlo and Seine seamounts, subtropical Northeast Atlantic. Deep Sea Res. Part II 56 (25), 2593–2605.

Bashmachnikov, I., Loureiro, C.M., Martins, A., 2013. Topographically induced circulation patterns and mixing over Condor seamount. Deep Sea Res. Part II 98, 38–51.

Böning, C.W., Behrens, E., Biastoch, A., Getzlaff, K., Bamber, J.L., 2016. Emerging impact of Greenland meltwater on deepwater formation in the North Atlantic Ocean. Nat. Geosci. 9 (7), 523–527.

Bonneau, L., Colin, C., Pons-Branchu, E., Mienis, F., Tisnérat-Laborde, N., Blamart, D., Elliot, M., Collart, T., Frank, N., Foliot, L., Douville, E., 2018. Imprint of holocene climate variability on cold-water coral reef growth at the SW Rockall Trough margin, NE Atlantic. Geochem. Geophys. Geosyst. 19, 2437–2452. https://doi.org/10.1029/2018GC007502.

Braga-Henriques, A., Porteiro, F.M., Ribeiro, P.A., De Matos, V., Sampaio, Í., Ocaña, O., Santos, R.S., 2013. Diversity, distribution and spatial structure of the cold-water coral fauna of the Azores (NE Atlantic). Biogeosciences 10 (6), 4009–4036.

Buhl-Mortensen, L., Vanreusel, A., Gooday, A.J., Levin, L.A., Priede, I.G., Buhl-Mortensen, P., Gheerardyn, H., King, N.J., Raes, M., 2010. Biological structures as a source of habitat heterogeneity and biodiversity on the deep ocean margins. Mar. Ecol. 31, 21–50. https://doi.org/10.1111/j.1439-0485.2010.00359.x.

Cascão, I., Domokos, R., Lammers, M.O., Marques, V., Domínguez, R., Santos, R.S., Silva, M.A., 2017. Persistent Enhancement of Micronekton Backscatter at the Summits of Seamounts in the Azores. Front. Mar. Sci. 4, 25. https://doi.org/10.3389/fmars.2017.00025.

Cathalot, C., Van Oevelen, D., Cox, T.J., Kutti, T., Lavaleye, M., Duineveld, G., Meysman, F.J., 2015. Cold-water coral reefs and adjacent sponge grounds: hotspots of benthic respiration and organic carbon cycling in the deep sea. Front. Mar. Sci. 2, 37.

Chu, J.W., Nephin, J., Georgian, S., Knudby, A., Rooper, C., Gale, K.S., 2019. Modelling the environmental niche space and distributions of cold-water corals and sponges in the Canadian northeast Pacific Ocean. Deep Sea Res. Part I 151, 103063.
Colin, C., Frank, N., Copard, K., Douville, E. (2010). Neodymium isotopic composition of deep-sea corals from the NE Atlantic: implications for past hydrological changes during the Holocene. Quat. Sci. Rev. 29 (19–20), 2509–2517. doi: 10.1016/j.quascirev.2010.05.012.
Colin, C., Tisnérat-Laborde, N., Mienis, F., Collart, T., Pons-Branchu, E., Dubois-Dauphin, Q., Frank, N., Dapoigny, A., Ayache, M., Swingedouw, D., Dutay, J.-C., Eynaud, F., Debret, M., Blamart, D., Douville, E., 2019. Millennial-scale variations of the Holocene North Atlantic mid-depth gyre inferred from radiocarbon and neodymium isotopes in cold water corals. Quat. Sci. Rev. 211, 93–106.
Cyr, F., van Haren, H., Mienis, F., Duineveld, G., Bourgault, D., 2016. On the influence of cold-water coral mound size on flow hydrodynamics, and vice versa. Geophys. Res. Lett. 43 (2), 775–783.
Davies, A.J., Wisshak, M., Orr, J.C., Murray Roberts, J., 2008. Predicting suitable habitat for the cold-water coral *Lophelia pertusa* (Scleractinia). Deep Sea Res. Part I 55 (8), 1048–1062.
Davies, A.J., Duineveld, G.C.A., Lavaleye, M.S.S., Bergman, M.J.N., van Haren, H., Roberts, J.M., 2009. Downwelling and deep-water bottom currents as food supply mechanisms to the cold-water coral *Lophelia pertusa* (Scleractinia) at the Mingulay Reef Complex. Limnol. Oceanogr. 54 (2), 620–629.
Davies, A.J., Guinotte, J.M., 2011. Global habitat suitability for framework-forming cold-water corals. PLoS One 6 (4), e18483.
De Clippele, L.H., Gafeira, J., Robert, K., Hennige, S., Lavaleye, M.S., Duineveld, G.C.A., Huvenne, V.A.I., Roberts, J.M., 2017. Using novel acoustic and visual mapping tools to predict the small-scale spatial distribution of live biogenic reef framework in cold-water coral habitats. Coral Reefs 36(1), 255–268.
De Clippele, L.H., van der Kaaden, A.-S., Maier, S.R., de Froe, E., Roberts, J.M., 2021. Biomass mapping for an improved understanding of the contribution of cold-water coral carbonate mounds to C and N cycling. Front. Mar. Sci. 8, 721062 https://doi.org/10.3389/fmars.2021.721062.
De Froe, E., Rovelli, L., Glud, R.N., Maier, S.R., Duineveld, G.C., Mienis, F., Lavaleye, M., van Oevelen, D., 2019. Benthic oxygen and nitrogen exchange on a cold-water coral reef in the North-East Atlantic Ocean. Front. Mar. Sci. 6, 665. https://doi.org/10.3389/fmars.2019.00665.
de Froe, E., Maier, S.R., Horn, H.G., Wolff, G.A., Blackbird, S., Mohn, C., Schultz, M., van der Kaaden, A.-S., Cheng, C.H., Wubben, E., van Haastregt, B., Moller, E.F., Lavaleye, M., Soetaert, K., Reichart, G.-J., van Oevelen, D., 2022. Hydrography and food distribution during a tidal cycle above a cold-water coral mound. Deep-Sea Res. 189, 103854.
Debreu, L., Vouland, C., Blayo, E., 2008. AGRIF: adaptive grid refinement in Fortran. Comput. Geosci. 31, 8–13. https://doi.org/10.1016/j.cageo.2007.01.009.
Dubois-Dauphin, Q., Colin, C., Elliot, M., Dapoigny, A., Douville, E., 2019. Holocene shifts in sub-surface water circulation of the North-East Atlantic inferred from Nd isotopic composition in cold-water corals. Mar. Geol. 410, 135–145. https://doi.org/10.1016/j.margeo.2019.01.004.
Duineveld, G.C., Lavaleye, M.S., Bergman, M.J., De Stigter, H., Mienis, F., 2007. Trophic structure of a cold-water coral mound community (Rockall Bank, NE Atlantic) in relation to the near-bottom particle supply and current regime. Bull. Mar. Sci. 81 (3), 449–467.
Dullo, W.C., Flögel, S., Rüggeberg, A., 2008. Cold-water coral growth in relation to the hydrography of the Celtic and Nordic European continental margin. Mar. Ecol. Prog. Ser. 371, 165–176.
Durski, S.M., Glenn, S.M., Haidvogel, D.B., 2004. Vertical mixing schemes in the coastal ocean: comparison of the level 2.5 Mellor-Yamada scheme with an enhanced version of the K profile parameterization. J. Geophys. Res. 109, C01015. https://doi.org/10.1029/2002JC001702.
Egbert, G.D., Erofeeva, S.Y., 2002. Efficient inverse modeling of barotropic ocean tides. J. Atmos. Oceanic Tech. 19 (2), 183–204.
Egbert, G.D., Ray, R.D., 2000. Significant dissipation of tidal energy in the deep ocean inferred from satellite altimeter data. Nature 405 (6788), 775–778.
Eisele, M., Frank, N., Wienberg, C., Hebbeln, D., López Correa, M., Douville, E., Freiwald, A., 2011. Productivity controlled cold-water coral growth periods during the last glacial off Mauritania. Mar. Geol. 280, 143–149. https://doi.org/10.1016/j.margeo.2010.12.007.
Flögel, S., Dullo, W.C., Pfannkuche, O., Kiriakoulakis, K., Rüggeberg, A., 2014. Geochemical and physical constraints for the occurrence of living cold-water corals. Deep Sea Res. Part II 99, 19–26.
Frajka-Williams, E., Ansorge, I.J., Baehr, J., Bryden, H.L., Chidichimo, M.P., Cunningham, S.A., Danabasoglu, G., Dong, S., Donohue, K.A., Elipot, S., Heimbach, P., Holliday, N.P., Hummels, R., Jackson, L.C., Karstensen, J., Lankhorst, M., Le Bras, I.A., Lozier, M.S., McDonagh, E.L., Meinen, C.S., Mercier, H., Moat, B.I., Perez, R.C., Piecuch, C.G., Rhein, M., Srokosz, M.A., Trenberth, K.E., Bacon, S., Forget, G., Goni, G., Kieke, D., Koelling, J., Lamont, T., McCarthy, G.D., Mertens, C., Send, U., Smeed, D.A., Speich, S., van den Berg, M., Volkov, D., Wilson, C., 2019. Atlantic meridional overturning circulation: observed transport and variability. Front. Mar. Sci. 6, 260. https://doi.org/10.3389/fmars.2019.00260.
Frederiksen, R., Jensen, A., Westerberg, H., 1992. The distribution of the scleractinian coral *Lophelia pertusa* around the Faroe Islands and the relation to internal tidal mixing. Sarsia 77 (2), 157–171.
Genin, A., 2004. Bio-physical coupling in the formation of zooplankton and fish aggregations over abrupt topographies. J. Mar. Syst. 50 (1-2), 3–20.
Genin, A., Dower, J.F., 2007. Seamount plankton dynamics. In: Pitcher, T.J., Morato, T., Hart, P.J.B., Clark, M.R., Haggan, N., Santos, R.S. (Eds.), Seamounts: Ecology, Fisheries and Conservation. Blackwell Publishing, Oxford, pp. 85–100.
Good, S.A., Martin, M.J., Rayner, N.A., 2013. EN4: quality controlled ocean temperature and salinity profiles and monthly objective analyses with uncertainty estimates. J. Geophys. Res. Oceans 118, 6704–6716. https://doi.org/10.1002/2013JC009067.
Hátún, H., Payne, M.R., Beaugrand, G., Reid, P.C., Sandø, A.B., Drange, H., Hansen, B., Jacobsen, J.A., Bloch, D., 2009a. Large bio-geographical shifts in the north-eastern Atlantic Ocean: from the subpolar gyre, via plankton, to blue whiting and pilot whales. Prog. Oceanogr. 80 (3-4), 149–162.
Hátún, H., Lohmann, K., Matei, D., Jungclaus, J.H., Pacariz, S., Bersch, M., Gislason, A., Ólafsson, J., Reid, P.C., 2016. An inflated subpolar gyre blows life toward the northeastern Atlantic. Prog. Oceanogr. 147, 49–66. https://doi.org/10.1016/j.pocean.2016.07.009.
Hátún, H., Olsen, B., Pacariz, S., 2017. The dynamics of the North Atlantic subpolar gyre introduces predictability to the breeding success of kittiwakes. Front. Mar. Sci. 4, 123.
Hátún, H., Payne, M.R., Jacobsen, J.A., 2009b. The North Atlantic subpolar gyre regulates the spawning distribution of blue whiting (*Micromesistius poutassou*). Can. J. Fish. Aquat. Sci. 66 (5), 759–770.
Hátún, H., Sandø, A.B., Drange, H., Hansen, B., Valdimarsson, H., 2005. Influence of the Atlantic subpolar gyre on the thermohaline circulation. Science 309 (5742), 1841–1844.
Hebbeln, D., Portilho-Ramos, R.d.C., Wienberg, C., Titschack, J., 2019. The fate of cold-water corals in a changing world: a geological perspective. Front. Mar. Sci. 6, 119. doi: 10.3389/fmars.2019.00119.
Hennige, S.J., Larsson, A.I., Orejas, C., Gori, A., De Clippele, L.H., Lee, Y.C., Jimeno, G., Georgoulas, K., Kamenos, N.A., Roberts, J.M., 2021. Using the Goldilocks Principle to model coral ecosystem engineering. Proc. R. Soc. B 288 (1956), 20211260.
Holliday, N.P., Cunningham, S.A., Johnson, C., Gary, S.F., Griffiths, C., Read, J.F., Sherwin, T., 2015. Multidecadal variability of potential temperature, salinity, and transport in the eastern subpolar North Atlantic. J. Geophys. Res. Oceans 120, 5945–5967. https://doi.org/10.1002/2015JC010762.
Johnson, C., Sherwin, T., Smythe-Wright, D., Shimmield, T., Turrell, W., 2010. Wyville Thomson Ridge Overflow Water: Spatial and temporal distribution in the Rockall Trough. Deep Sea Res. I 57, 1153–1162. https://doi.org/10.1016/j.dsr.2010.07.006.
Johnson, C., Sherwin, T., Cunningham, S., Dumont, E., Houpert, L., Holliday, N.P., 2017. Transports and pathways of overflow water in the Rockall Trough. Deep Sea Res. Part I 122, 48–59.
Johnson, C., Inall, M., Gary, S., Cunningham, S.A., 2020. Significance of climate indices to benthic conditions across the Northern North Atlantic and Adjacent Shelf Seas. Front. Mar. Sci. 7, 2. https://doi.org/10.3389/fmars.2020.00002.
Juva, K., Flögel, S., Karstensen, J., Linke, P., Dullo, W.C., 2020. Tidal dynamics control on cold-water coral growth: a high-resolution multivariable study on eastern Atlantic cold-water coral sites. Front. Mar. Sci. 7, 132.
Kazanidis, G., Henry, L.-A., Vad, J., Johnson, C., De Clippele, L.H., Roberts, J.M., 2021. Sensitivity of a cold-water coral reef to interannual variability in regional oceanography. Divers. Distrib. 27, 1719–1731.
Kenyon, N.H., Akhmetzhanov, A.M., Wheeler, A.J., van Weering, T.C.E., de Haas, H., Ivanov, M.K., 2003. Giant carbonate mud mounds in the southern Rockall Trough. Mar. Geol. 195 (1–4), 5–30. https://doi.org/10.1016/S0025-3227(02)00680-1.
Khripounoff, A., Caprais, J.C., Le Bruchec, J., Rodier, P., Noel, P., Cathalot, C., 2014. Deep cold-water coral ecosystems in the Brittany submarine canyons (Northeast Atlantic): Hydrodynamics, particle supply, respiration, and carbon cycling. Limnol. Oceanogr. 59 (1), 87–98.
Klein, B., Siedler, G., 1989. On the origin of the Azores Current. J. Geophys. Res. Oceans 94 (C5), 6159–6168.
Large, W.G., McWilliams, J.C., Doney, S.C., 1994. Oceanic vertical mixing: a review and a model with a nonlocal boundary layer parameterization. Rev. Geophys. 32, 363–403.
Ledwell, J.R., Montgomery, E.T., Polzin, K.L., St. Laurent, L.C., Schmitt, R.W., Toole, J. M., 2000. Evidence for enhanced mixing over rough topography in the abyssal ocean. Nature 403(6766), 179–182.
Lim, A., Wheeler, A.J., Price, D.M., O'Reilly, L., Harris, K., Conti, L., 2020. Influence of benthic currents on cold-water coral habitats: a combined benthic monitoring and 3D photogrammetric investigation. Sci. Rep. 10 (1), 1–15.
Lozier, M.S., Owens, W.B., Curry, R.G., 1995. The climatology of the North Atlantic. Prog. Oceanogr. 36 (1), 1–44.
Maier, S.R., Mienis, F., de Froe, E., Soetaert, K., Lavaleye, M., Duineveld, G., Beauchard, O., van der Kaaden, A.-S., Koch, B.P., van Oevelen, D., 2021. Reef communities associated with 'dead' cold-water coral framework drive resource retention and recycling in the deep sea. Deep Sea Res. Part I Oceanogr. Res. Pap. 175, 103574 https://doi.org/10.1016/j.dsr.2021.103574.
McClain, C.R., 2007. Seamounts: identity crisis or split personality? J. Biogeogr. 34 (12), 2001–2008.
McGrath, T., Kivimäe, K., Tanhua, T., Cave, R.R., McGovern, E., 2012. Inorganic carbon and pH levels in the Rockall Trough 1991–2010. Deep Sea Res., Part I 68, 79–91. https://doi.org/10.1016/j.dsr.2012.05.011.
Merrifield, M.A., Holloway, P.E., Johnston, T.S., 2001. The generation of internal tides at the Hawaiian Ridge. Geophys. Res. Lett. 28 (4), 559–562.
Mienis, F., van Weering, T., de Haas, H., de Stigter, H., Huvenne, V., Wheeler, A., 2006. Carbonate mound development at the SW Rockall Trough margin based on high resolution TOBI and seismic recording. Mar. Geol. 233 (1–4), 1–19. https://doi.org/10.1016/j.margeo.2006.08.003.
Mienis, F., De Stigter, H.C., White, M., Duineveld, G., De Haas, H., Van Weering, T.C.E., 2007. Hydrodynamic controls on cold-water coral growth and carbonate-mound development at the SW and SE Rockall Trough Margin, NE Atlantic Ocean. Deep Sea Res. Part I 54 (9), 1655–1674.

Mienis, F., de Stigter, H., de Haas, H., van Weering, T.C.E., 2009. Near-bed particle deposition and resuspension in a cold-water coral mound area at the Southwest Rockall Trough margin, NE Atlantic. Deep Sea Res., Part I 56 (6), 1026–1038. https://doi.org/10.1016/j.dsr.2009.01.006.

Mienis, F., Duineveld, G.C.A., Davies, A.J., Lavaleye, M.M.S., Ross, S.W., Seim, H., Bane, J., van Haren, H., Bergman, M.J.N., de Haas, H., Brooke, S., van Weering, T.C. E., 2014. Cold-water coral growth under extreme environmental conditions, the Cape Lookout area, NW Atlantic. Biogeosciences 11, 2543–2560. https://doi.org/10.5194/bg-11-2543-2014.

Mienis, F., Bouma, T.J., Witbaard, R., van Oevelen, D., Duineveld, G.C.A., 2019. Experimental assessment of the effects of cold-water coral patches on water flow. Mar. Ecol. Prog. Ser. 609, 101–117. https://doi.org/10.3354/meps12815.

Mohn, C., Gary, S., van Oevelen, D. (2019). Data set for initializing and forcing of high-resolution local area model implementations in two ATLAS case study areas, Rockall Bank and Condor Seamount [Data set]. Zenodo. doi: 10.5281/zenodo.3582932.

Mohn, C., Rengstorf, A., White, M., Duineveld, G., Mienis, F., Soetaert, K., Grehan, A., 2014. Linking benthic hydrodynamics and cold-water coral occurrences: a high-resolution model study at three cold-water coral provinces in the NE Atlantic. Prog. Oceanogr. 122, 92–104.

Mohn, C., White, M., Denda, A., Erofeeva, S., Springer, B., Turnewitsch, R., Christiansen, B., 2021. Dynamics of currents and biological scattering layers around Senghor Seamount, a shallow seamount inside a tropical Northeast Atlantic eddy corridor. Deep Sea Res. Part I 171, 103497.

Montero-Serrano, J.-C., Frank, N., Colin, C., Wienberg, C., Eisele, M., 2011. The climate influence on the mid-depth Northeast Atlantic gyres viewed by cold-water corals. Geophys. Res. Lett. 38 (19), n/a–n/a.

Morato, T., González-Irusta, J.-M., Dominguez-Carrió, C., Wei, C.-L., Davies, A., Sweetman, A.K., Taranto, G.H., Beazley, L., García-Alegre, A., Grehan, A., Laffargue, P., Murillo, F.J., Sacau, M., Vaz, S., Kenchington, E., Arnaud-Haond, S., Callery, O., Chimienti, G., Cordes, E., Egilsdottir, H., Freiwald, A., Gasbarro, R., Gutiérrez-Zárate, C., Gianni, M., Gilkinson, K., Wareham Hayes, V.E., Hebbeln, D., Hedges, K., Henry, L.-A., Johnson, D., Koen-Alonso, M., Lirette, C., Mastrototaro, F., Menot, L., Molodtsova, T., Durán Muñoz, P., Orejas, C., Pennino, M.G., Puerta, P., Ragnarsson, S.Á., Ramiro-Sánchez, B., Rice, J., Rivera, J., Roberts, J.M., Ross, S.W., Rueda, J.L., Sampaio, Í., Snelgrove, P., Stirling, D., Treble, M.A., Urra, J., Vad, J., Oevelen, D., Watling, L., Walkusz, W., Wienberg, C., Woillez, M., Levin, L.A., Carreiro-Silva, M., 2020. Climate-induced changes in the suitable habitat of cold-water corals and commercially important deep-sea fishes in the North Atlantic. Glob. Chang. Biol. 26 (4), 2181–2202.

Nikurashin, M., Legg, S., 2011. A mechanism for local dissipation of internal tides generated at rough topography. J. Phys. Oceanogr. 41 (2), 378–395.

Nikurashin, M., Vallis, G.K., Adcroft, A., 2013. Routes to energy dissipation for geostrophic flows in the Southern Ocean. Nat. Geosci. 6 (1), 48–51.

O'Brien, C.L., Spooner, P.T., Wharton, J.H., Papachristopoulou, E., Dutton, N., Fairman, D., Garratt, R., Li, T., Pallottino, F., Stringer, F., Thornalley, D.J.R., 2021. Exceptional 20th century shifts in deep-sea ecosystems are spatially heterogeneous and associated with local surface ocean variability. Front. Mar. Sci. 8, 663009 https://doi.org/10.3389/fmars.2021.663009.

Orejas, C., Gori, A., Rad-Menéndez, C., Last, K.S., Davies, A.J., Beveridge, C.M., Sadd, D., Kiriakoulakis, K., Witte, U., Roberts, J.M., 2016. The effect of flow speed and food size on the capture efficiency and feeding behaviour of the cold-water coral *Lophelia pertusa*. J. Exp. Mar. Biol. Ecol. 481, 34–40.

Osterloff, J., Nilssen, I., Järnegren, J., van Engeland, T., Buhl-Mortensen, P., Nattkemper, T.W., 2019. Computer vision enables short- and long-term analysis of *Lophelia pertusa* polyp behaviour and colour from an underwater observatory. Sci. Rep. 9, 6578. https://doi.org/10.1038/s41598-019-41275-1.

Palma, C., Lillebø, A.I., Borges, C., Souto, M., Pereira, E., Duarte, A.C., de Abreu, M.P., 2012. Water column characterisation on the Azores platform and at the sea mounts south of the archipelago. Mar. Pollut. Bull. 64 (9), 1884–1894.

Penny Holliday, N., Pollard, R.T., Read, J.F., Leach, H., 2000. Water mass properties and fluxes in the Rockall Trough, 1975–1998. Deep-Sea Res. 47 (7), 1303–1332.

Petit, T., Lozier, M.S., Josey, S.A., Cunningham, S.A., 2020. Atlantic deep water formation occurs primarily in the Iceland Basin and Irminger Sea by local buoyancy forcing. Geophys. Res. Lett. 47, e2020GL091028. doi: 10.1029/2020GL091028.

Puerta, P., Johnson, C., Carreiro-Silva, M., Henry, L.-A., Kenchington, E., Morato, T., Kazanidis, G., Rueda, J.L., Urra, J., Ross, S., Wei, C.-L., González-Irusta, J.M., Arnaud-Haond, S., Orejas, C., 2020. Influence of Water Masses on the Biodiversity and Biogeography of Deep-Sea Benthic Ecosystems in the North Atlantic. Front. Mar. Sci. 7, 239. https://doi.org/10.3389/fmars.2020.00239.

Purser, A., Larsson, A.I., Thomsen, L., van Oevelen, D., 2010. The influence of flow velocity and food concentration on *Lophelia pertusa* (Scleractinia) zooplankton capture rates. J. Exp. Mar. Biol. Ecol. 395 (1–2), 55–62.

Radach, G., Moll, A., 2006. Review of the three-dimensional ecological modelling related to the north sea shelf system – part 2: Model Validation and Data Needs. Oceanogr. Mar. Biol. – Ann. Rev. 44, 1–60.

Rakka, M., Orejas, C., Maier, S.R., Van Oevelen, D., Godinho, A., Bilan, M., Carreiro-Silva, M., 2020. Feeding biology of a habitat-forming antipatharian in the Azores Archipelago. Coral Reefs 39 (5), 1469–1482.

Rakka, M., Maier, S.R., Van Oevelen, D., Godinho, A., Bilan, M., Orejas, C., Carreiro-Silva, M., 2021. Contrasting metabolic strategies of two co-occurring deep-sea octocorals. Sci. Rep. 11 (1), 1–12.

Rengstorf, A.M., Mohn, C., Brown, C., Wisz, M.S., Grehan, A.J., 2014. Predicting the distribution of deep-sea vulnerable marine ecosystems using high-resolution data: Considerations and novel approaches. Deep Sea Res. Part I 93, 72–82.

Roberts, J.M., Cairns, S.D., 2014. Cold-water corals in a changing ocean. Curr. Opin. Environ. Sustain. 7, 118–126.

Roberts, J.M., Wheeler, A.J., Freiwald, A., 2006. Reefs of the deep: the biology and geology of cold-water coral ecosystems. Science 312 (5773), 543–547.

Roberts, J.M., Davies, A.J., Henry, L.A., Dodds, L.A., Duineveld, G.C.A., Lavaleye, M.S.S., Maier, C., van Soest, R.W.M., Bergman, M.J.N., Hühnerbach, V., Huvenne, V.A.I., Sinclair, D.J., Watmough, T., Long, D., Green, S.L., van Haren, H., 2009. Mingulay reef complex: an interdisciplinary study of cold-water coral habitat, hydrography and biodiversity. Mar. Ecol. Prog. Ser. 397, 139–151.

Rovelli, L., Attard, K.M., Bryant, L.D., Flögel, S., Stahl, H., Roberts, J.M., Linke, P., Glud, R.N., 2015. Benthic O2 uptake of two cold-water coral communities estimated with the non-invasive eddy correlation technique. Mar. Ecol. Prog. Ser. 525, 97–104.

Rovelli, L., Carreiro-Silva, M., Attard, K.M., Rakka, M., Dominguez-Carrió, C., Bilan, M., Blackbird, S., Morato, T., Wolff, G.A., Glud, R.N., 2022. Benthic O2 uptake by coral gardens at the Condor seamount (Azores). Mar. Ecol. Prog. Ser. 688, 19–31.

Sampaio, Í., Freiwald, A., Mora, F.P., Menezes, G., Carreiro-Silva, M., 2019. Census of Octocorallia (Cnidaria: Anthozoa) of the Azores (NE Atlantic) with a nomenclature update. Zootaxa 4550 (4), 451–498.

Santos, M., Moita, M.T., Bashmachnikov, I., Menezes, G.M., Carmo, V., Loureiro, C.M., Mendonça, A., Silva, A.F., Martins, A., 2013. Phytoplankton variability and oceanographic conditions at Condor seamount, Azores (NE Atlantic). Deep Sea Res. Part II 98, 52–62.

Schulz, K., Soetaert, K., Mohn, C., Korte, L., Mienis, F., Duineveld, G., van Oevelen, D., 2020. Linking large-scale circulation patterns to the distribution of cold water corals along the eastern Rockall Bank (northeast Atlantic). J. Mar. Syst. 212, 103456 https://doi.org/10.1016/j.jmarsys.2020.103456.

Shchepetkin, A.F., McWilliams, J.C., 2005. The Regional Ocean Modeling System (ROMS): a split-explicit, free-surface, topography following-coordinate oceanic model. Ocean Model. 9, 347–404.

Shimeta, J.E.F.F., Jumars, P.A., 1991. Physical mechanisms and rates of particle capture by suspension-feeders. Oceanogr. Mar. Biol. Annu. Rev. 29, 191–257.

Siemer, J.P., Machín, F., González-Vega, A., Arrieta, J.M., Gutiérrez-Guerra, M.A., Pérez-Hernández, M.D., Fraile-Nuez, E., 2021. Recent trends in SST, Chl-a, productivity and wind stress in upwelling and open ocean areas in the Upper Eastern North Atlantic Subtropical Gyre. J. Geophys. Res.: Oceans 126(8), e2021JC017268.

Signorini, S.R., Franz, B.A., McClain, C.R., 2015. Chlorophyll variability in the oligotrophic gyres: mechanisms, seasonality and trends. Front. Mar. Sci. 2, 1–11. https://doi.org/10.3389/fmars.2015.00001.

Soetaert, K., Mohn, C., Rengstorf, A., Grehan, A., van Oevelen, D., 2016. Ecosystem engineering creates a direct nutritional link between 600-m deep cold-water coral mounds and surface productivity. Sci. Rep. 6, 35057. https://doi.org/10.1038/srep35057.

Spooner, P.T., Thornalley, D.J., Oppo, D.W., Fox, A.D., Radionovskaya, S., Rose, N.L., Mallett, R., Cooper, E., Roberts, J.M., 2020. Exceptional 20th century ocean circulation in the northeast Atlantic. Geophys. Res. Lett. 47(10), e2020GL087577.

Srokosz, M.A., Bryden, H.L., 2015. Observing the Atlantic Meridional Overturning Circulation yields a decade of inevitable surprises. Science 348 (6241), 1255575.

Sundahl, H., Buhl-Mortensen, P., Buhl-Mortensen, L., 2020. Distribution and Suitable Habitat of the Cold-Water Corals *Lophelia pertusa*, *Paragorgia arborea*, and *Primnoa resedaeformis* on the Norwegian Continental Shelf. Front. Mar. Sci. 7, 213. https://doi.org/10.3389/fmars.2020.00213.

Sweetman, A.K., Thurber, A.R., Smith, C.R., Levin, L.A., Mora, C., Wei, C.-L., Gooday, A. J., Jones, D.O.B, Rex, M., Yasuhara, M., Ingels, J., Ruhl, H.A., Frieder, C.A., Danovaro, R., Würzberg, L., Baco, A., Grupe, B.M., Pasulka, A., Meyer, K.S., Dunlop, K.M., Henry, L.-A., Roberts, J.M., 2017. Major impacts of climate change on deep-sea benthic ecosystems. Elem. Sci. Anth. 5, 4. doi: 10.1525/elementa.203.

Tempera, F., Giacomello, E., Mitchell, N.C., Campos, A.S., Braga Henriques, A., Bashmachnikov, I., Martins, A., Mendonça, A., Morato, T., Colaço, A., Porteiro, F.M., Catarino, D., Gonçalves, J., Pinho, M.R., Isidro, E.J., Santos, R.S., Menezes, G., 2012. 59 - Mapping condor seamount seafloor environment and associated biological assemblages (Azores, NE Atlantic). In: Harris, P.T., Baker, E.K. (Eds.), Seafloor Geomorphology as Benthic Habitat, Elsevier, pp. 807–818. ISBN 9780123851406. doi: 10.1016/B978-0-12-385140-6.00059-1.

Thyng, K.M., Greene, C.A., Hetland, R.D., Zimmerle, H.M., DiMarco, S.F., 2016. True colors of oceanography. Oceanography 29 (3), 10.

Van der Kaaden, A.S., Mohn, C., Gerkema, T., Maier, S.R., de Froe, E., van de Koppel, J., Rietkerk, M., Soetaert, K., van Oevelen, D., 2021. Feedbacks between hydrodynamics and cold-water coral mound development. Deep Sea Res. Part I: Oceanogr. Res. Pap. 178, 103641.

Van Haren, H., Mienis, F., Duineveld, G.C., Lavaleye, M.S., 2014. High-resolution temperature observations of a trapped nonlinear diurnal tide influencing cold-water corals on the Logachev mounds. Prog. Oceanogr. 125, 16–25.

Van Oevelen, D., Duineveld, G., Lavaleye, M., Mienis, F., Soetaert, K., Heip, C.H., 2009. The cold-water coral community as hotspot of carbon cycling on continental margins: a food-web analysis from Rockall Bank (northeast Atlantic). Limnol. Oceanogr. 54 (6), 1829–1844.

Van Soest, R.W.M., Lavaleye, M.S.S., 2005. Diversity and abundance of sponges in bathyal coral reefs of Rockall Bank, NE Atlantic, from boxcore samples. Mar. Biol. Res. 1 (5), 338–349. https://doi.org/10.1080/17451000500380322.

van Weering, T.C.E., de Haas, H., de Stigter, H.C., Lykke-Andersen, H., Kouvaev, I., 2003. Structure and development of giant carbonate mounds at the SW and SE Rockall Trough margins, NE Atlantic Ocean. Mar. Geol. 198 (1-2), 67–81.

Wagner, H., Purser, A., Thomsen, L., Jesus, C.C., Lundälv, T., 2011. Particulate organic matter fluxes and hydrodynamics at the Tisler cold-water coral reef. J. Mar. Syst. 85 (1–2), 19–29.

Wan, Z., She, J., Maar, M., Jonasson, L., Baasch-Larsen, J., 2012. Assessment of a physical-biogeochemical coupled model system for operational service in the Baltic Sea. Ocean Sci. 8 (4), 683–701.

Wang, G., Dewar, W.K., 2003. Meddy–seamount interactions: implications for the Mediterranean salt tongue. J. Phys. Oceanogr. 33 (11), 2446–2461.
White, M., Roberts, J.M., van Weering, T., 2007. Do bottom-intensified diurnal tidal currents shape the alignment of carbonate mounds in the NE Atlantic? Geo-Mar. Lett. 27, 391–397. https://doi.org/10.1007/s00367-007-0060-8.
White, M., Bashmachnikov, I., Arstegui, J., Martins, A., 2008. Physical processes and seamount productivity. In: Seamounts: Ecology, Fisheries & Conservation. Blackwell Publishing Ltd, Oxford, UK, pp. 62–84.
White, M., Dorschel, B., 2010. The importance of the permanent thermocline to the cold water coral carbonate mound distribution in the NE Atlantic. Earth Planet. Sci. Lett. 296 (3-4), 395–402.
White, M., Wolff, G.A., Lundälv, T., Guihen, D., Kiriakoulakis, K., Lavaleye, M., Duineveld, G., 2012. Cold-water coral ecosystem (Tisler Reef, Norwegian Shelf) may be a hotspot for carbon cycling. Mar. Ecol. Prog. Ser. 465, 11–23.
Wienberg, C., Titschack, J., 2017. Framework-forming scleractinian coldwater corals through space and time: a late Quaternary North Atlantic perspective. In: Rossi, S., Bramanti, L., Gori, A., Orejas Saco del Valle, C. (Eds.), Marine Animal Forests: The Ecology of Benthic Biodiversity Hotspots. Springer, Cham, pp., 699–732.
Wienberg, C., Titschack, J., Frank, N., De Pol-Holz, R., Fietzke, J., Eisele, M., Kremer, A., Hebbeln, D., 2020. Deglacial upslope shift of NE Atlantic intermediate waters controlled slope erosion and cold-water coral mound formation (Porcupine Seabight, Irish margin). Quat. Sci. Rev. 237, 106310.
Wilson, C.D., Boehlert, G.W., 2004. Interaction of ocean currents and resident micronekton at a seamount in the central North Pacific. J. Mar. Syst. 50 (1–2), 39–60.